Engineering Physics bachelor degree's Final Thesis

Design and implementation of an organic semi-transparent photovoltaic device

A 5-month thesis at the Group of Organic Nanostructured Photovoltaics, ICFO (Castelldefels, Barcelona, Spain)

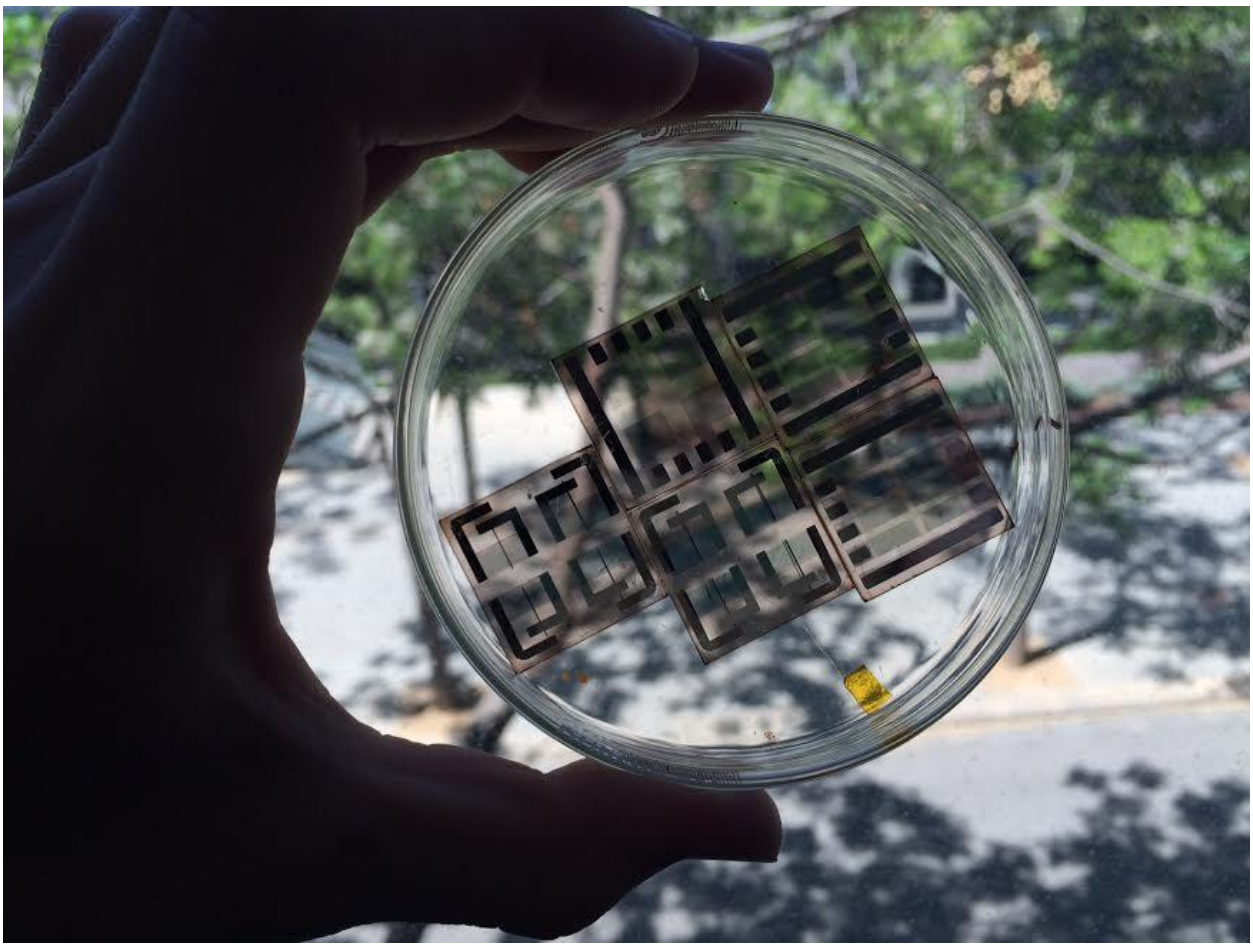

By Jordi Puig Ribas

Supervised by Paola Mantilla

Director: Jordi Martorell

Co-director: Joaquim Puigdollers

June 2016

SUMMARY

1. ABSTRACT

Organic polymeric solar cells require thin absorber layers due to intrinsic low exciton diffusion distances, thus showing low absorption of light. They are also characterized by having a low absorption peak, whose position lies in the near-infrared, slightly affecting the visible spectrum. By depositing thin silver layers of 10 nm for the back electrode, a semi-transparent organic solar cell can be created. Attractive outcomes could result from these devices, like solar cell windows that would remain visually transparent, while still collecting energy from the sun, or tandem polymeric solar cells. The formation of a non-homogeneous and discontinuous silver layer when depositing an ultra-thin film turns into a high resistivity electrode, therefore limiting the area that such devices can reach and the maximum power that the cell can offer. The goal of this bachelor thesis was to up-scale semi-transparent organic solar cells by characterizing the thin electrode conductivity and enhancing its charge collection using thick grid-like layers of silver. The cause for such high resistivity was confirmed by finding silver agglomerations of 30 nm in size, and a lower limit for its value was found by studying the silver bulk resistivity. The up-scaling losses were determined in terms of the increase in area, and charge-collecting grids were consequently tested. The building of organic solar cells by spin-coating and vapour depositions was proved functional on top of non-flat substrates with roughness of the order of 100 nm. Fill Factor enhancements were found by designing optimal grid structures compatible with highly transparent cells.

2. INTRODUCTION

2.1. Photovoltaics background

Human society's need for renewable, low-cost, sustainable and reachable energy sources has been increasingly growing for the last decades. It is expected that the global energy power demand will overcome a value of 71 TW by 2050. [1] In order to fulfil this expectation, seeking for candidate energy sources is obligatory nowadays. That said, one of the most obvious reliable large-scale source is the Sun. The energy reached every day by Sun's rays at the surface of our planet is huge: every hour, sunlight delivers the same amount of energy used by all humanity in one year. A power of 1kW/m^2 hits the Earth's surface when our star is in Zenith.[2] These facts offer us a solution to the global energy needs, through finding an efficient way of converting that power into, for example, electrical power: Photovoltaics.

Photovoltaics (PV) is the technology used to convert light into electricity, and solar cells are PV devices delivering current at a determinate voltage upon solar light exposure. They work using the "photovoltaic effect", a light-absorbing effect taking place in semiconductor materials. A solar cell is manufactured on transparent substrates (to let the light enter the device) carrying different layers: a photoactive semiconducting layer sandwiched between two electrodes. The photoactive layer, or just active layer, is the layer where the photovoltaic effect takes place: it absorbs the energy of an incident photon to excite an electron from its valence band (VB), and move it to the conduction band (CB) of such semiconducting material. This electron leaves a hole behind in the VB. The reason why the active layer is sandwiched by electrodes is the collection of such electron-hole (e-h) pair. Holes are modelled as positive electron charges and will be collected in the Anode, while electrons are collected in the Cathode. To let the light reach the active layer, at least one of the electrodes has to be transparent (or semi-transparent). But not all wavelengths of electromagnetic radiation will be converted into an electron-hole pair: as the electron has to be excited from the VB to the CB, only those photons having at least the energy difference between those bands (called the bandgap energy or E_G) will be absorbed. This means that only a specific range of wavelengths from Sun’s spectrum will be absorbed.

Once the e-h pair is created, it is then necessary to collect and separate them. The method to “harvest” these charge carriers is creating an electrical field, which can be done in the junction of the active layer with an electrode, or in the p-n junction within the active material (doping the semiconductor). At the point where electrons are collected in the Cathode and holes in the Anode, it is necessary to close the circuit and make electrons fill the holes through making them pass a consumer load, which generates current.

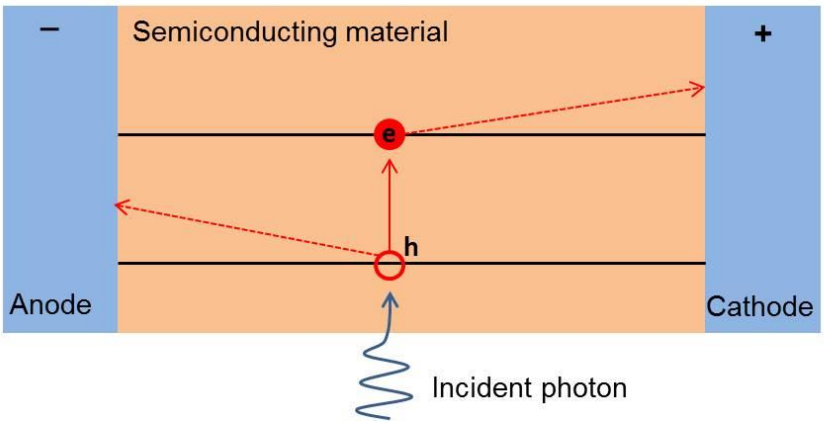

Figure 2.1. Generation of free charge carriers through the photovoltaic effect, and subsequent collection of such carriers by applying an external voltage in the electrodes.

2.2 Characterization of a solar cell

The common way to measure the performance of a solar cell is to put it under the illumination of a solar simulator, which radiates with the AM 1.5G solar spectrum (1000 W/m^2) at a temperature of 25ºC. The label AM 1.5G means *air mass 1.5 global,* which refers to the amount of air mass in Earth's atmosphere that the light has to travel through before reaching the surface, being 1.5G an air quantity 1.5 times larger than the one sun rays travel through at zenith. This is equivalent to simulate incident sunrays when the sun is at a zenith angle of 48º. This is shown in figure 2.2.[3] Once the cell is under this radiation, an increasing voltage is applied to the electrodes, and the resulting current flow produced by the cell, for each electric potential, is measured.

The expected I-V curve is similar to the typical diode curve, as current can only be allowed in one direction, starting only at the point where the applied voltage generates an electric field of enough magnitude to separate the e-h pairs, increasing then exponentially for higher applied voltages (see exponential dependence in Figure 2.3). To make the measurement more precise, the current density J (current per cell area) is measured instead of the current I.

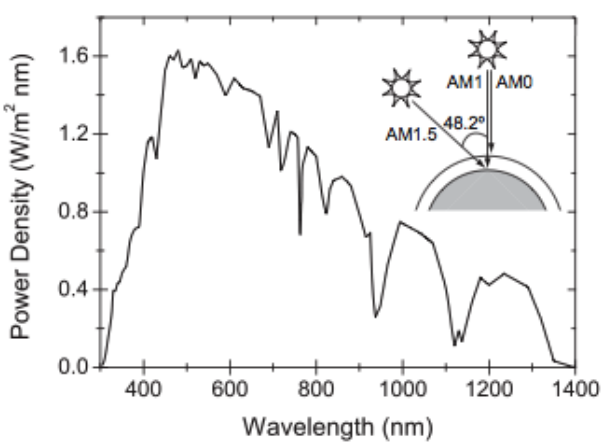

Figure 2.2. The AM 1.5G spectrum (graphic) and its equivalent sunrays incidence (cartoon).

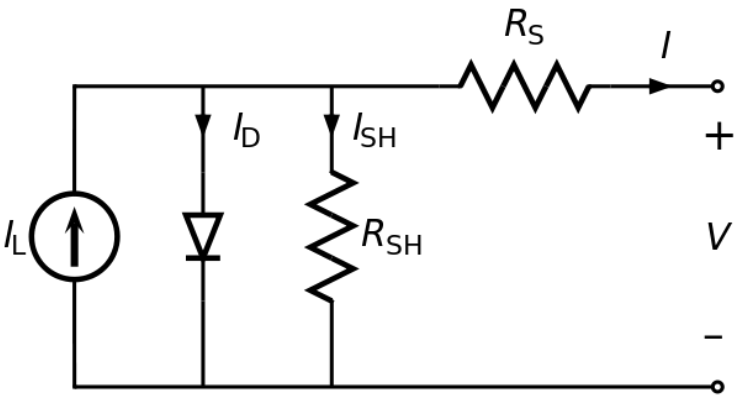

$$I = I_L - I_0 \left[exp \left[\frac{V + IR_s}{n\, V_t} \right] - 1 \right] - \frac{V + IR_s}{R_{SH}} \qquad (1)$$

Figure 2.3. Equivalent circuit (top) and IV equation (bottom) for a generic solar cell. I is the output current, I_L the photogenerated current, I_0 is the reverse saturation current of a diode, I_D is the diode current, R_{SH} and I_{SH} are the shunt resistance and current (representing the losses due to recombination), and R_s is the series resistance. V is the applied voltage, n is the diode's quality factor (from 0 to 1), and V_T is the thermal voltage. It is clear that the voltage dependence of the current is exponential with two adding linear factors.

From this J-V measurement, important performance parameters can be inferred. In order to get them, it is important to define the parameters:

- **J_{sc}**: Current density obtained when cell's electrodes are in short-circuit, under AM 1.5G solar illumination.
- **V_{oc}**: Voltage measured between cell's electrodes when they are in open-circuit and illuminated with AM 1.5G solar spectrum.

These parameters, multiplied by each other, give the maximum power that could ideally be obtained from the cell (P_{MAX}). The comparison between this ideal power and the actual maximum power point of the cell, obtained for some voltage (V_{MPP}) and some current (J_{MPP}) of the cell's J-V response, is made by a parameter called Fill Factor (FF), which is a measure of the whole quality of the cell.

$$FF = \frac{J_{mpp} \times V_{mpp}}{J_{sc} \times V_{oc}} \qquad (2)$$

This parameters are graphically shown in figure 2.4.

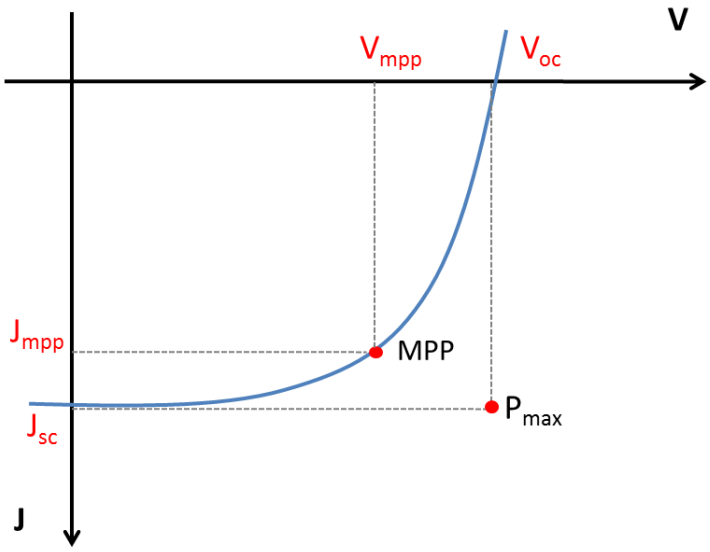

Figure 2.4. A typical J-V curve from a solar cell's measurement under illumination, with indication of the open-circuit voltage ($\mathbf{V_{oc}}$) and the short-circuit current density ($\mathbf{J_{sc}}$), together with the maximum power. The maximum power point (MPP) is also shown, with its corresponding voltage (V_{mpp}) and current density (J_{mpp}). The area enclosed by the square made by the MPP with the axes gives the actual maximum power of the cell. The area of the square made by Voc and Jsc gives the maximum ideal power that could be obtained. The quotient given by the small area over the big area gives the Fill Factor.

Another interesting number is the power conversion efficiency (PCE or η). It is the ratio of the power density delivered by the cell on its MPP to the incident radiation power received by the cell per unit area (P_{INC}). In other words, it measures the amount of light power that is transformed into electrical power by the cell.

$$FF = \frac{J_{mpp} \times V_{mpp}}{P_{inc}} = \frac{FF \times J_{sc} \times V_{oc}}{P_{inc}} \qquad (3)$$

Another typical characterization of a PV device is the external quantum efficiency (EQE). This measure tells which percentage of the total incident photons is actually exciting an electron that is correctly harvested and transformed into current, for each wavelength. The device is not illuminated by the Sun's spectrum, but by monochromatic illumination, and the J_{sc} is measured while stepwise changing the wavelength of the incident monochromatic light. An EQE curve is shown in figure 2.5.

Integrating the whole curve over the wavelengths and taking into account the different photon flux for each wavelength in the solar spectrum, one gets the total J_{sc}.

$$Jsc = \int EQE(\lambda) \cdot P_{sun}(\lambda) \cdot \frac{e \cdot \lambda}{h \cdot c} d\lambda \qquad (4)$$

Here, e represents the elementary charge, h the constant of Planck and c the speed of light.
This value can be higher than the one calculated from J-V measurement, as individual wavelength illumination does not saturate the device as much as AM 1.5G solar spectrum illumination.

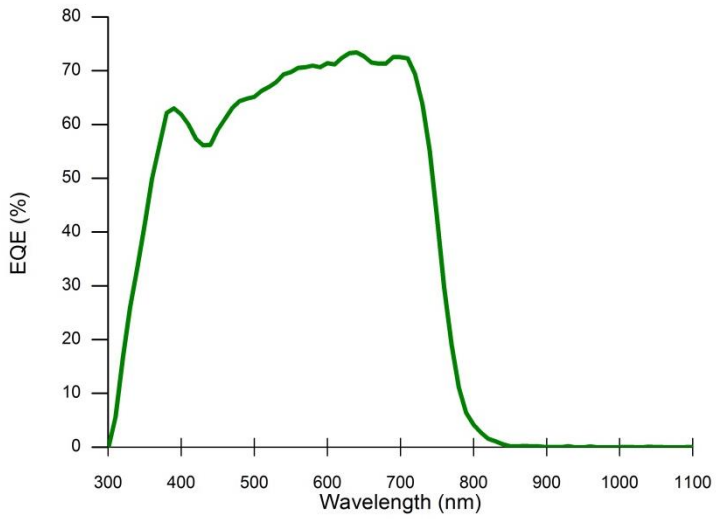

Figure 2.5. External Quantum Efficiency of an organic solar cell. It shows the amount of photons that are efficiently transformed into current for each wavelength. Only a certain range of wavelengths is absorbed by the device.

2.3. Organic Photovoltaics

Conventional PV devices use doped inorganic crystalline silicon as the absorbing layer. With a low absorption coefficient, active layers in the order of 200 μm have to be made, and efficiencies of 18.5% are typically obtained by monocrystalline Si devices that are produced industrially.[4] But silicon-based solar cells are expensive to fabricate, as well as time and energy-consuming because of different steps during the fabrication process. This is one of the main reasons why researchers have looked for other materials having different characteristics. An alternative are organic semiconducting materials like polymers, as used in organic polymeric solar cells (PSC). Even though some of the highest PCE's reached in the lab have been between 10% and 11%, they offer many advantages in comparison to the crystalline silicon. The polymeric material used for the active layer can be solution-processed, which eases the

fabrication while avoiding vacuum deposition methods, and can be tuned easily by changing the concentration or the chemical configuration for an optimized performance. In fact, important parameters like conductivity, E_G or solubility can be actually tailored. Other interesting characteristics of such materials are their wide chemical diversity, their low production cost, and their high absorption allowing thinner layers of active material. In the following, some other interesting characteristics of organic (or polymeric) solar cells will be discussed, as well as some limitations or challenges they present.

In silicon-based PV, the free charge carriers generated by the incident light are separated automatically by the electric field at the heterojunction. But for organic photovoltaics (OPV), charge carriers are not free: after leaving a hole behind, the photo-excited electron still feels Coulombic attraction to it, so they both cannot move freely from each other. This effect is due to the low dielectric constant (ε_r) that organic materials intrinsically have in relation to silicon, which makes Coulomb attraction increase (see formula nº 5).

$$F = \frac{1}{4\pi\varepsilon_0\varepsilon_r} \cdot \frac{q_1 q_2}{r^2} \qquad (5)$$

The resulting Coulombically-bound electron-hole pair is called an exciton.

It takes energy to overcome this attraction, and because of their closeness there is an increased risk of recombination: the electron comes back to the hole and they cannot be harvested and converted into electrical current. This is one of the main reasons why efficiency is lower than in silicon-based cells. Another limitation of organic light-absorbing materials is exciton's low diffusion length and mobility. This makes OPV need thin absorbing layers to lower the distance that the charge carriers have to travel before finding a junction to be collected, otherwise they recombine and don't contribute to the electrical current. But thin layers limit the total light absorption and thus the cell's current and efficiency. However, this restriction is partially compensated by the high absorption of organic materials. The result are OPV devices of typical absorbing layer's thicknesses of 100nm. This saves material and allows for lightweight, flexible or even semi-transparent solar cells, as well as for a roll-to-roll industrial fabrication process.

Even though the organic absorber is still a semiconductor, the model of valence and conduction band does not apply anymore. For inorganic semiconducting active layers, excited photons generated free charge carriers as long as they had at least the same energy as the material's bandgap (if photons carry more energy than E_G, the excess energy is lost via thermalization and the photon is still absorbed). However, the energy levels in organic materials are governed by molecular orbitals, so photoexcitation moves an electron from the highest occupied molecular

orbital (HOMO) to the lowest unoccupied molecular orbital (LUMO), and generates an exciton between those orbitals. The energy difference between these is still referred to as E_G. The simplest way to dissociate the bound pair into free charges, is depositing a bilayer heterojunction composed of two organic materials with offset energy levels, presented by Tang in 1986.[5] This interface created between two organic materials is the way to create charge carriers out of the photogenerated excitons, basically thanks to the energy offset between their respective frontier orbitals. This orbital energy difference makes the material with the lowest ionization potential act as a donor, and the one with the highest electron affinity act as an acceptor. So the charge transfer (occurring at the donor-acceptor interface) results in one hole in the donor's HOMO orbital, and one electron in the acceptor's LUMO orbital. They still cannot be considered as free charge carriers because they are still attracted by Coulombic interaction, but can be finally separated by the difference in work function of the electrodes that sandwich the heterojunction. Electrons travel through the acceptor to the low work function electrode (Cathode), and holes travel through the donor to the high work function electrode (Anode). All this steps are depicted in figure 2.5.

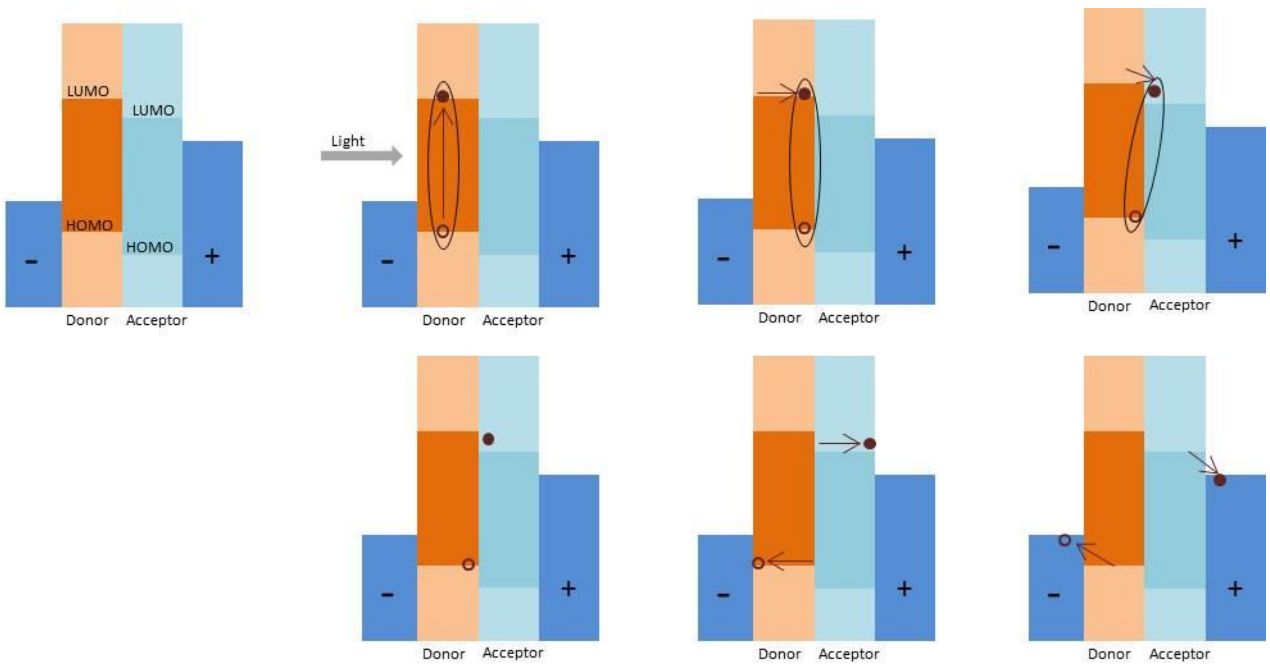

Figure 2.5. The subsequent steps creating free charge carriers in a bilayer heterojunction solar cell: 1. Absorption, 2. Exciton diffusion to the interface, 3. Charge transfer, 4. Charge separation, 5. Charge transport, 6. Charge collection.

2.4. OPV device configuration

Exciton's diffusion length in organic semiconductors is limited to about 10nm due to their low mobility and short lifetime before recombination.[6-7] It is because of this that only those excitons that have been created close to the organic-organic interface in the photoactive layer will be efficiently separated into charge carriers. This fact makes the organic bilayer structure loose a large amount of photocurrent, as only a small percentage of the photogenerated excitons will yield charge carriers. The solution for this problem was found in 1995[8] and it lays on the intrinsic tendency of polymer materials to phase separate at nanometric scale when mixing them. By solution mixing donor and acceptor materials and then depositing them as the active layer (i.e. *bulk heterojunction*), the interface surface between both materials is increased and spread throughout the bulk and ensures quantitative dissociation of excitons. By then sandwiching this mixed layer (commonly called *blend*) with the electrodes, a larger number of free charges are collected and a more efficient solar cell is created (see figure 2.6).

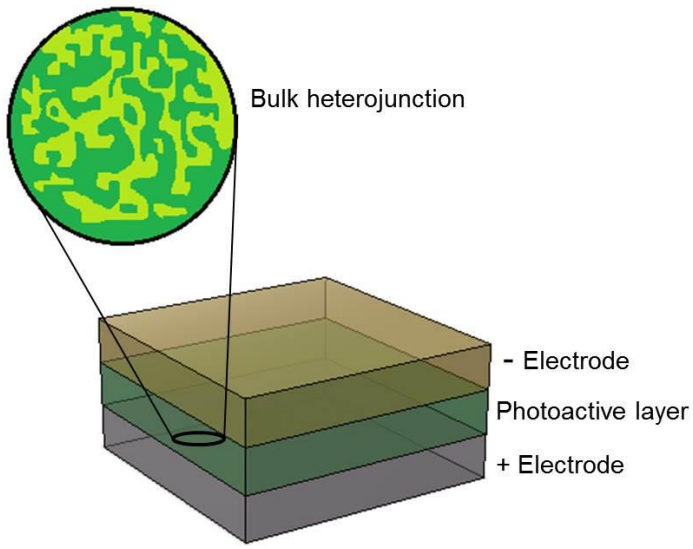

Figure 2.6. Representation of the nanometric phase separation of the donor and acceptor materials in the blend, used as an ubiquitous interface throughout the layer, and sandwiched by the electrodes

Usually bulk heterojunction polymer solar cells are built on a transparent substrate (mainly glass) coated with a conductive and transparent electrode material (called the front electrode). In most cases the material used is ITO (indium tin oxide) due to its transparency and conductivity. The following layers, forming the solar cell structure, can follow two different kinds of configuration: direct or inverted.

In direct configuration, ITO works as the anode, and is followed by an electron blocking layer (EBL) which usually is made of poly(3,4-ethylenedioxythiophene):poly(styrenesulfonate) (PEDOT:PSS). Electron blocking layers (and the complementary case, hole blocking layers) let easily pass one species of charge carriers, while they block the other, so they facilitate electron-hole separation. After the PEDOT:PSS layer, the blend (active layer) is deposited, and followed

by a TiO_2, that works as a hole blocking layer (HBL). On top of it, a low work function metal is deposited as the opaque cathode (called back electrode), being Ca or Al commonly used materials. However, the PEDOT:PSS EBL and the low work function metal cathode are detrimental to long-term device performance.[9] The inverted configuration shows an improved ambient stability while offering processing advantages by avoiding one vacuum process.

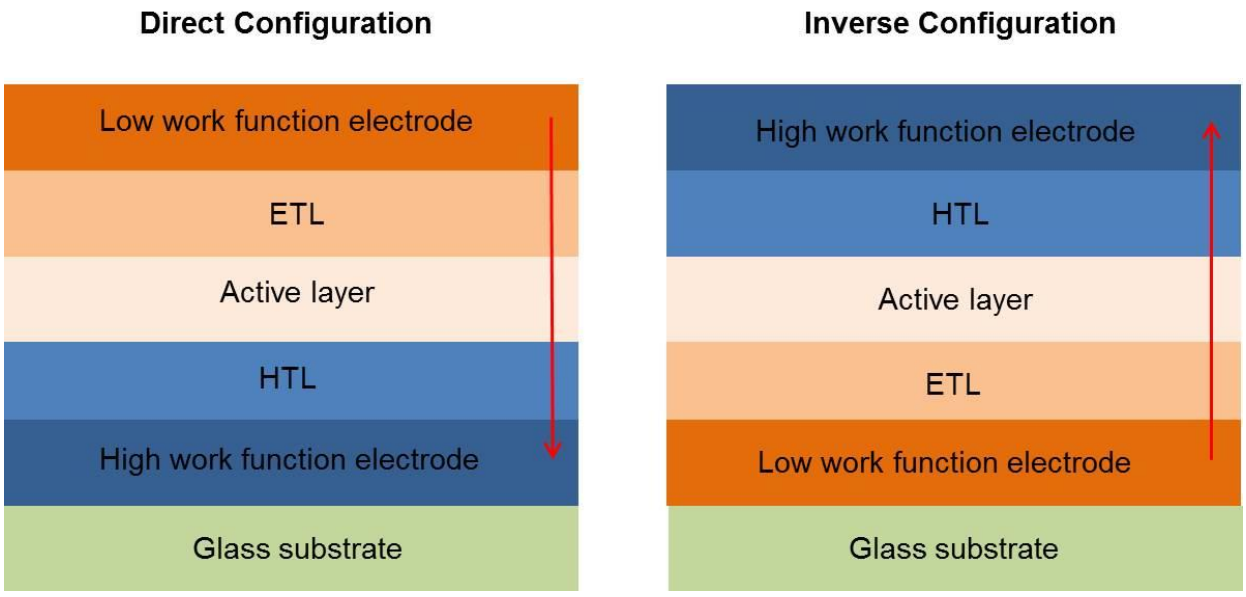

Figure 2.7. Visualization of the different order in cell's layers and current flow direction (red arrows) for the direct and inverse configurations.

For inverted configurations, glass substrate coated with ITO is also used, but now ITO works as the anode: the current flows in the opposite direction as in direct configurations. Zinc oxide (Z_nO) is then used as an HBL and as a wetting layer to smoothen the surface, easing the following deposition of the blend. Then an EBL of molybdenum oxide (MoO_3) is deposited, followed by the high work function electrode, which is usually made out of an air stable material such as Au or Ag.

2.5. Semi-transparent Photovoltaic Devices

As mentioned before, one of the multiple applications of OPV comes from their allowance for semi-transparent appearance. In fact, they are the only ones permitting active layers to be thin enough to transmit a good amount of the visible electromagnetic spectrum. However, this is not enough for the whole cell to be semi-transparent, as in usual OPV devices the first electrode (coated on top of the glass substrate) was already transparent, but not the second one (the one on top of all the layers, including: substrate, first electrode, transport layers and blend). So for

this application, the top electrode layer also has to be semi-transparent. The way to do it is by designing a thinner layer for that electrode, of the order of 10nm. But, as an obvious consequence, coating the electrode with less amount of material will change the conductivity and reduce the device performance. Another basic consequence of semi-transparency is the loss of internal reflection of light. When light enters the active layer in an opaque cell, it can be either absorbed (creating thus electrical current) or transmitted. The transmitted light will then reach the opaque top electrode and be reflected, entering the active layer again and so exciting more electrons. This feature can help reach higher PCE's, and semi-transparent OPV devices cannot count on it, as that internal optical reflection is highly reduced.

In addition, the production process of such devices requires a larger number of steps, increasing the experimental difficulties (see detailed experimental process in section 3.2).

Despite all this difficulties, it is an interesting research area aiming for applications such as polymer tandem photovoltaic devices[10] or photovoltaic windows. Keeping in mind the increasingly large presence of windows in buildings there is nowadays, the amount of energy that could be collected out of them is huge.

2.6. Objective of the theses: upscaling

Increasing cell's area is an important feature for semi-transparent OPV, and for its main applications like photovoltaic windows. When upscaling these devices, they present increasingly decaying performance for larger areas. It is deduced that this could be due to the loss of conductivity in the electrodes, as they are both semi-transparent, so they have to be thinner (especially the back electrode). This would increase the resistance and, when upscaling, the charge carriers would have to travel a larger distance through this resistance-increased electrode before reaching the contacts. As a consequence, a significant reduction in the FF is obtained.

I have done this project during a 5-month stay at ICFO (The Institute of Photonic Sciences) in the Organic Nanostructured Photovoltaics group. My research has been based on building semi-transparent organic solar cells, studying the performance's decay when increasing their size and improving their performance when upscaling them, through reducing conductivity losses at the electrodes when increasing the cell's size.

Within this research group, there have been studies of the upscaling of semi-transparent OPV devices by connecting different cells in series, that is, doing a physical connection between one cell's anode and the next cell's cathode, and so on. This permits to build a solar cell module (atmosphere-protected encapsulated final device) with a larger area without having increased the individual cells' area, thus preventing performance losses. It is also a way to increase V_{oc}, as different voltages add when they are connected in series. The production method used to

connect polymeric cells in series is laser scribing, and it is based on sequential cuts of selected layers within the device performed with lasers, in order to stablish serial connections between the solar cells. The method basically consists of three cuts: P1, P2, P3. P1 scribes the front electrode and its HBL. Then the absorbing layer is deposited and P2 scribes it without harming the front electrode and the HBL. After, the EBL and the back electrode are deposited, and P3 scribes them and the absorbing layer without harming the front electrode and its HBL, again. The “dead area” is the zone between P1 and P3. The direction of the current is shown by the blue arrows (opposite of electron’s direction). P1 and P3 are needed to stop the current continuing in the corresponding electrodes, and P2 is used to connect both electrodes, creating a series connection between the sub cells divided by the “dead area”.Laser scribing method is depicted in figure 2.8.

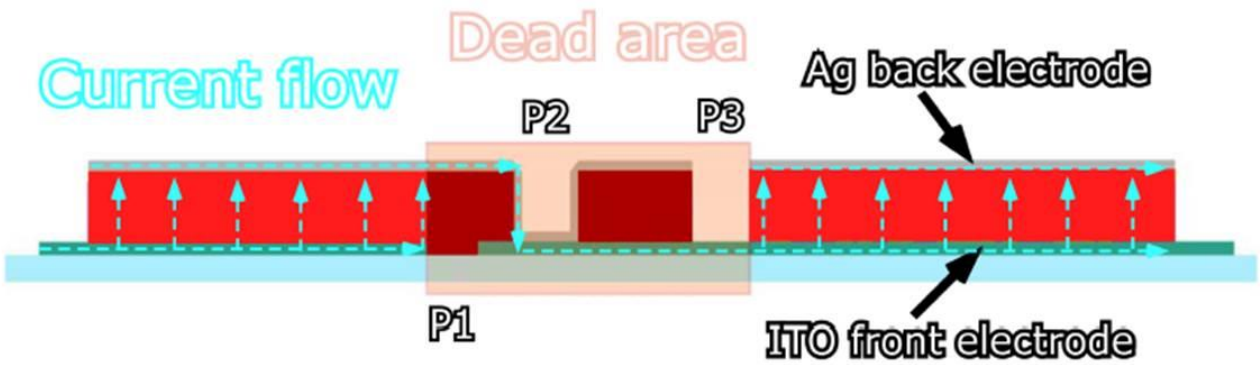

Figure 2.8. Image taken from Elias Rehmann’s theses on “Semi-Transparent Organic Solar Cells, Connected in Series by Laser Scribing” (Organic Nanostructured Photovoltaics, ICFO). It shows the three different steps done to create a cell made of sub cells connected in series for the inverse configuration.

Besides from leaving a “dead area” zone that visually affects the transparency of the module and does not produce any current, this method has been proved inefficient within the group. Apparently, the laser evaporation is not leaving a “clean” cut in the polymer, but instead is melting some of it and leaving agglomerations of material in the sides of the laser scribe. When later coating a thin silver layer to short-circuit the material that is out of the cut with the bottom electrode, these agglomerations are too big to allow for a uniform deposition and act as a wall in the layer, complicating the contact between the sides of the “wall” . This does not allow the series connection of the cells. A Scanning Electron Microscopy image of such agglomerations is shown in figure 2.9.

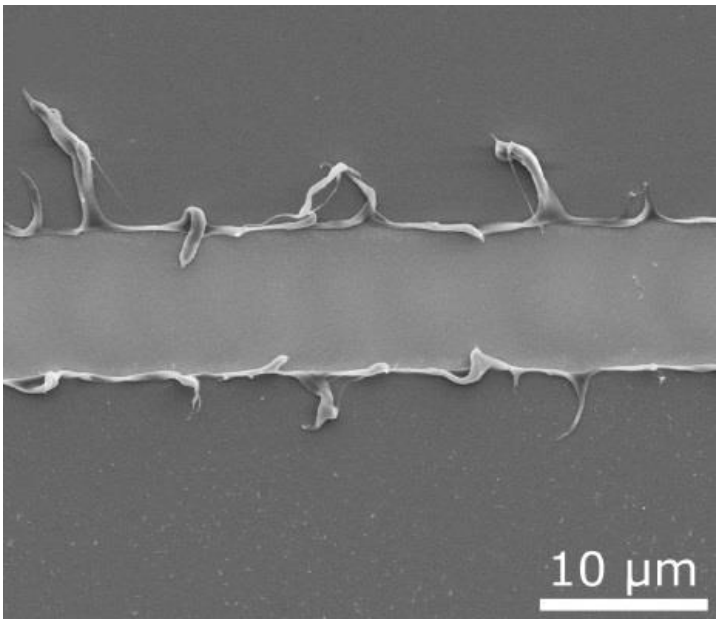

Figure 2.9. SEM image of the P2 scribing through the absorber layer. The protrusions appearing at the edges of the cut are agglomerations of melted polymer.

While looking for ways to solve or improve this method, upscaling of the individual cells should also be done taking into account the necessity to reduce the amount of series connections and consequently, the amount of “dead areas” and losses due to laser scribing.

My objective is to study how the performance losses scale in semi-transparent OPV when increasing the area, how the electrical conductivity is affected when depositing thinner electrodes, and to consequently design a proper device structure enhancing the FF of larger devices, without deteriorating transparency. This will be attempted through studying the differences in measurements under illumination when varying cell’s areas, varying electrode’s thicknesses, and adding thick silver grid structures within the electrode layers to collect charges and reduce the resistance. All of these studies will be compared to other better-performing devices like opaque solar cells or small-area semi-transparent devices.

3. METHODOLOGICAL BACKGROUND

3.1. Experimental methods

To enable the making of all the experiments and characterizations needed for this project, many different machines, setups and recipes had to be used. In the following, all these experimental methods will be shortly described.

The different experimental methods or setups that were used are the following:

- Fume hood: it is a ventilation device in a closet-like appearance, preventing the exposure or inhalation of toxic gases and dusts while allowing working with them. It was used to clean liquid or substrate containers, magnets for mixing chemicals, and other utilities with different solvents and prevent their inhalation. It was also used to deposit the ZnO layer.

Figure 3.1. Fume hood from the Organic Nanostructured Photovoltaics' lab.

- Glovebox: it is a sealed chamber or box where one can manipulate substrates, deposit layers or store samples or chemicals in a desired atmosphere. Part of the box is transparent and there are big gloves built into the It features several gloves, resistant to different solvents, for the user to manipulate the objects inside without breaking the atmosphere. During most of the production process and after it, samples were placed in the glovebox in a N_2 environment (1 atm) to avoid oxidation and further degradation.

Figure 3.2. One of the gloveboxes in the Organic Nanostructured Photovoltaics lab.

- Ultrasonication bath device: it is a device exposing its open chamber to ultrasounds. It is used as a really common and precise way of cleaning object surfaces, by placing the samples in a small sample container, filling it with different solvents, and exposing it to ultrasounds using the device.

Figure 3.3. Ultrasonication bath device from the chemistry lab in ICFO.

- UV lamp: it is a device used to remove organic remnants from the substrates after being cleaned with a solvent, by exposing them to UV light for some minutes in a closed chamber.

- Spin-coater: it is a device which rotates substrates at high speeds, used as a way to deposit thin uniform layers of solution-processed materials in flat surfaces. It has a small substrate-holder where one can place the object and fix it. After fixing the substrate (usually by vacuum), the machine makes it rotate. Before or while it starts rotating, the solution can be applied in the centre of the substrate for a static or dynamic spin-coating, respectively. The high speed rotation spreads the solution uniformly over the surface. Spin-coating was used for the ZnO, PFN and blend layer depositions.

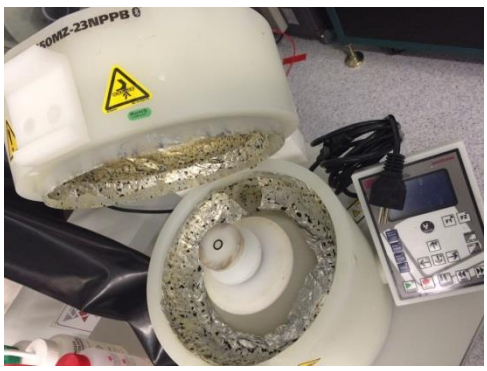

Figure 3.4. Spin-coater WS-650MZ-23NPP, Laurell Technologies. This one was used inside the fume hood to deposit the ZnO layer.

- Deposition evaporator: it is a system to perform deposition of thin inorganic materials and metallization. Under a high vacuum atmosphere, it heats the material at a determinate rate until it evaporates and gets deposited in the substrate's surface in a uniform way (due to the rotation of the substrate holder) because of physical condensation of such gas when contacting the substrate. Placing a sensor next to the holder and controlling the evaporation rate allows for an accurate control of the deposited layer's thickness. In addition, this process does not require a flat sample's surface (as the gas will ideally hit any rotating surface uniformly), and so allows for the placing of masks in the substrates, covering the parts where the new layer is not desired. This method was used for the deposition of the EBL of MoO_3 and the back silver electrode.

Figure 3.5. Vacuum vapor deposition machine's outside (left) and inside (right) views. In the inside view there is the substrate holder in the top part and the different vapor sources in the bottom part.

- Solar simulator: high power lamp illuminating a small area with AM 1.5G spectrum. Samples were placed within that area and contacted in the electrodes to measure solar cell's parameters.

Figure 3.7. Sun 3000 solar simulator (Abet Technologies).

- Source-measurement unit: while illuminating the devices, electrodes were contacted and plugged into a software-driven source-measurement unit (SourceMeter, Keithley). It was used to deliver a desired voltage in the electrodes while measuring the obtained current during illumination. The software used to obtain the data is the Tracer2, Abet Technologies software.

- Chiller: a chiller was used to cool the substrates to -5ºC before vapour depositions of very thin Ag layers (see section 3.2.5). When using it, the evaporator substrate holder was not able to rotate, affecting thus the uniformity of the depositions.

- Hot plate: electronic device with a metallic flat plate allowing the temperature and surface magnetic field control. It was used to anneal the substrates after some layer deposition, and also to heat dissolutions and mix them, by stirring a magnet inside the dissolution container by the changing magnetic field.

Figure 3.6. Hot plates inside the glovebox.

- Etching: chemical procedure used to erase a determinate layer from a surface. It was used at some points to eliminate some part of the ITO coating from the glass substrates. It is possible to maintain the layer in the desired parts by covering and protecting them from the chemicals with a mask or with tape. The recipe to erase ITO consisted in covering the surface with Zinc powder, and then dropping HCl (2M) on top. After 10 minutes, when cleaning the Zinc from the substrates, the ITO had been removed.

- Sol-gel process: method used to produce solid materials from small molecules, typically used for metal oxides. In our case it was used to deposit the ZnO HBL. It involves converting monomers into a solution, that acts as a precursor, and then depositing it and annealing the substrate for the dissolvent liquids to evaporate, leaving a set of discrete particles or network polymers in the surface.

- Four-point measurement: it is a useful and precise way to calculate sheet resistances of thin layers by contacting the material with 4 electrodes: 2 to introduce a current, and 2 to measure the voltage difference induced by the current. It eliminates the contact resistance from the measurement, providing an accurate impedance value.

- UV-Vis transmission spectroscope: it is a device which illuminates the solar cell with different wavelengths and measures the transmission using a light sensor at the other side of the beam incidence. It is a useful way to characterize cell's transparency.

- AFM (Atomic Force Mycroscopy): it is a high resolution scanning probe microscopy used to characterize surfaces at a resolution of fractions of a nanometer. A thin tip is precisely controlled by piezoelectric elements and it moves close to the surface, while measuring the force between the probe and the sample. It allows calculating the roughness and other interesting parameters of the surface.

3.2. Basic sample fabrication and measurement processes

In this section, the subsequent steps followed in the production of the OPV samples will be described, as well as the characterization processes and the ways in which the methods in the previous section have been used. The different recipes and materials have been created, adopted or improved by the Organic Nanostructured Photovoltaics group at ICFO, and at some point of the project some fabrication steps or even materials had to be changed or substituted due to discovery updates, experimental needs, or research group requirements. The aim of this section is to make an accurate description of the different methods that future sections will refer to.

The OPV device configuration used for this project was the inverse, using ITO as the front electrode collecting electrons, ZnO as the HBL, the polymer PCE10 and the fullerene PC71BM for the blend, MoO3 as the EBL, and silver (Ag) for the back electrode collecting holes.

The **basic process** took usually two or three days and included the following steps:

- Produce ZnO
- Produce Blend
- Acquire substrate: glass with ITO
- Clean substrate (ultrasonicate)
- UV treatment
- Deposit ZnO precursor
- Deposit organic absorber blend
- Deposit MoO3 and Ag
- Measurements

At a specific point of the project, a new fabrication recipe was adopted by our group due to recent discoveries providing improvements against device degradation. Even though the process is pretty similar, a new layer is deposited (PFN layer) after the ZnO, the blend proportion is changed as well as the organic solvent, and layer's thicknesses are also slightly changed.

The **degradation-improved process** took also two or three days and included:

- Produce ZnO
- Produce Blend
- Produce PFN
- Aquire substrate: glass with ITO
- Clean substrate (ultrasonicate)
- UV treatment
- Deposit ZnO precursor
- Deposit PFN
- Deposit organic absorber blend
- Deposit MoO3 and Ag
- Measurements

3.2.1. Substrate with ITO

The substrates I used consisted of quadratic glass slides covered with electrically conductive and transparent ITO (135nm, 15Ω/sq). They had a thickness of 1.1 mm and an area of 2.5x2.5 cm^2. The ITO layer was not covering the whole surface, but followed a two-stripe pattern with a stripe thickness of 3mm each.

Before starting the deposition of layers, a cleaning procedure was followed to make sure the surface was free of impurities at the start of the process. It consisted on immersing the substrates in a series of ultrasonication baths:

- Cleaning soap, 5 minutes
- Deionized water, 3 minutes
- Acetone, 5 minutes
- Deionized water, 3 minutes
- Ethanol, 5 minutes
- Deionized water, 3 minutes
- Methanol, 5 minutes

They were finally dried with a blow pistol of N_2, put in a Petri dish (previously cleaned with Isopropanol and dried), and put for 10 minutes under UV radiation for a complete cleaning.

After these steps, the substrates were stored inside the glovebox until the HBL coating.

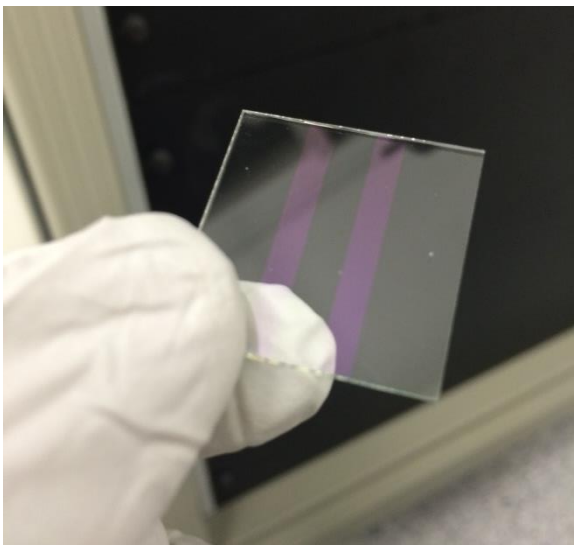

Figure 3.8. Picture of an ITO 2-stripe coated substrate. The “purple” areas are the ITO stripes. Although they are transparent, notice this picture has been taken at the right angle to capture ITO’s reflection to show the coating pattern.

3.2.2. ZnO hole blocking layer

The HBL consisted of zinc oxide (ZnO), and was produced by a sol-gel process: a liquid precursor was applied to the substrate and then it was annealed at high temperature.

I fabricated the precursor in ICFO's Chemical Lab, following the recipe used by our group, which consisted on mixing Zinc acetate, methanol, and ethanolamine. It resulted in a 0.15M solution. After mixing the chemicals, it was stirred (400 rpm) at temperature (60ºC) for at least 4h, which was usually done overnight.

The coating was done in a spin-coater inside the fume hood, dropping the precursor statically and spinning the substrate at 6000 rpm during 45 seconds with an acceleration of 10000 rpm/s. 100µl of precursor were needed for each substrate. After coating, they were annealed in the hotplate at 170ºC during 10 minutes, to transform the precursor into zinc oxide. Finally it was stored in the glovebox for further sample manipulations.

3.2.3. PFN layer (degradation-improved process)

This layer was only applied and created in the degradation-improved process. For that case, it was deposited after the ZnO layer and before the blend. Changfeng Han *et al* [11] demonstrated that a bilayer made of ZnO and *poly[(9,9-bis(3-(N,N-dimethylamino)propyl)-2,7-fluorene)-alt-2,7-(9,9-dioctyfluorene)]* (PFN) enhanced electron transport and energy level alignment. Quan Liu, from the Organic Nanostructured Photovoltaics group at ICFO, was working on degradation of OPV and adopted this bilayer recipe. As it was improving cell's performance and not influencing my research, at a point in my project I also adopted it (see section 4.7).

I produced the PFN by mixing solid dust-like PFN material with methanol and acetic acid in a 0.2M dissolution for PFN. After mixing the chemicals, stirring (200rpm) at room temperature was done overnight.

The coating was performed in a different spin-coater placed inside the glovebox, dropping 180µl of the solution statically and then rotating the sample at 3000 rpm for 30 seconds. Finally it was put in a hot plate inside the glovebox at 60ºC for 1 minute. After letting it cool down, the active layer could be deposited.

3.2.4. Organic absorber

Starting with this step (or PFN in the degradation recipe), the devices were kept under protective nitrogen atmosphere inside the glovebox to avoid contact with oxygen or humidity.

A layer of around 100nm of the light-absorbing polymeric blend was deposited using the spin-coater inside the glovebox, with a posterior rest of 1 hour in high vacuum for the layer to dry without any impurity being stuck (using the vapour deposition machine only for its vacuum pumps).

The blend's recipe for the standard procedure involved mixing the chemically modified fullerene $PC_{71}BM$ *([6,6]-phenyl C71-butyric acid methyl ester)*, which worked as the acceptor, and the polymer PCE10 *(Poly[4,8-bis(5-(2-ethylhexyl)thiophen-2-yl)benzo[1,2-b;4,5-b']dithiophene-2,6-diyl-alt-(4-(2-ethylhexyl)-3-fluorothieno[3,4-b]thiophene-)-2-carboxylate-2-6-diyl])*, working as the donor. The proportions of PCE10:$PC_{71}BM$ were respectively 1:1.5. The mix was then dissolved in Chlorobenzene *(C_6H_5Cl)* and stirred (200rpm) at 60ºC in the hot plate overnight. In the day after, the addition of a little amount of DIO *(1,8-Diiodooctane)* was done and followed by 1 hour of stirring. Finally, it was ready to be deposited dynamically in the spin-coater at 2000 rpm for 45 seconds, and then put to rest under vacuum.

The blend's recipe for the degradation-improved procedure involved different steps that still cannot be divulgated.

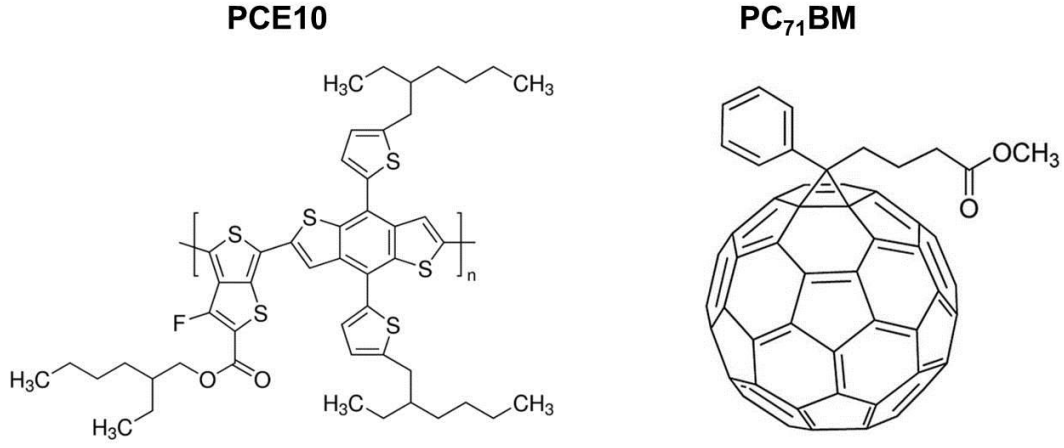

Figure 3.9. PCE10 and $PC_{71}BM$'s molecular structure.

3.2.5. MoO3 electron blocking layer and Ag electrode

The devices were then placed in the evaporator's sample holder, which could fit 6 different samples, thus limitating the amount of cells per experiment. They were fixed together with their shadow masks, permitting the deposition only in the desired area. The overlap between the two electrodes gives the active device area, and thus the masks were used to design the number of cells in a substrate and their areas (by creating different silver overlaps for each ITO stripe). This is depicted in figure 3.13. The holder was then placed in the evaporator device, and the whole cavity was put under a vacuum of 10^{-5} bar. When the vacuum was reached, the different layers were deposited. From this point, there were two different ways to deposit the layers: one for the opaque cells and another for the semi-transparent ones:

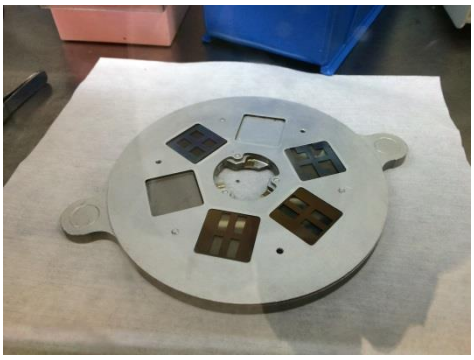

Figure 3.10. shadow masks and substrates fixed in the holder.

- Opaque cells: the EBL of MoO_3 was deposited with holder rotation at a rate of 0.6 Armstrongs per second (Å/s) with a thickness of 5 nm (10 nm for the degradation-improved method). Then the Ag electrode was deposited at a rate of 1 Å/s with a thickness of 100 nm, also with rotation. Cells were contacted directly from the silver electrode when measuring. To better contact the ITO lying at the bottom of the substrate when measuring, Ag was also deposited on the areas previously cleaned of blend with acetone.

- Semi-transparent cells: a 5 nm layer of MoO_3 (10 nm for the degradation-improved method) was deposited in the same way as the opaque cell process. Then the Ag electrode was deposited, this time with a thickness of only 10 nm, thus absorbing much less light. When such small amount of Ag is deposited at room temperature, silver agglomerations will form, creating a non-homogeneous layer, with electrode overlap (and so, active cell area) only in the agglomerations and not in the rest of the desired area. To avoid this, a chiller was switched on to lower the substrate temperature to -5 ºC. This makes the Ag particles have less energy and mobility through the surface, preventing their interaction and reducing the agglomerations. However, this setup made it impossible to rotate the holder during the evaporation, so

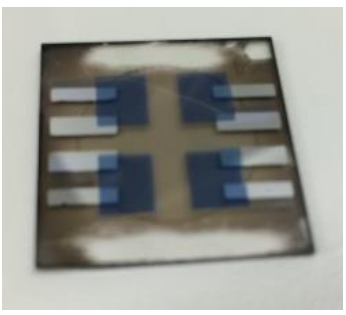

Figure 3.11. Finalized sample with two zones of cleaned blend (top and bottom white spots) to enable the ITO contact.

thicknesses were not equally distributed over the substrates, as they are at different distances from the evaporating source when put in the holder.

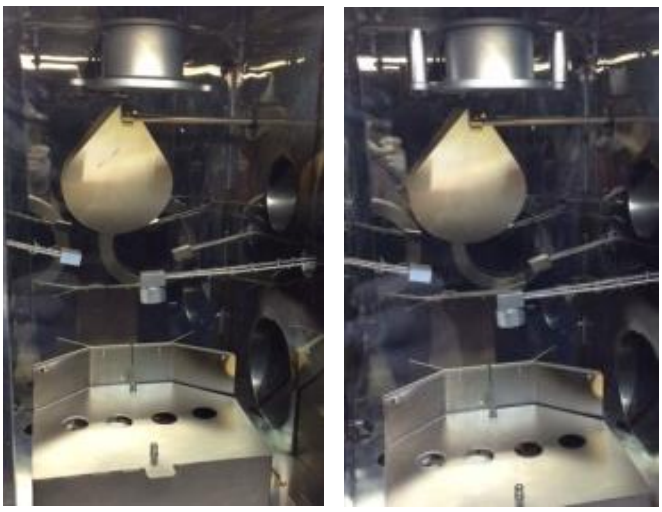

Figure 3.12. Evaporator's cavity with (right) and without (left) rotation set ups. The setup for cooling does not allow for rotation because the holder is fixed by two magnets.

Figure 3.13 illustrates the modified cell structure with the semi-transparent back electrode. It is not recommended to contact the thin electrode for measuring, as it was done in opaque cells, because it could harm such thin layer. To avoid doing so, a thick Ag layer (150 nm) was deposited, on top of the thin silver and outside the active cell area defined by the overlap between ITO and thin Ag. Finally, to protect the electrode, another transparent layer of MoO_3 was deposited on top of the thin silver (100 nm, with rotation).

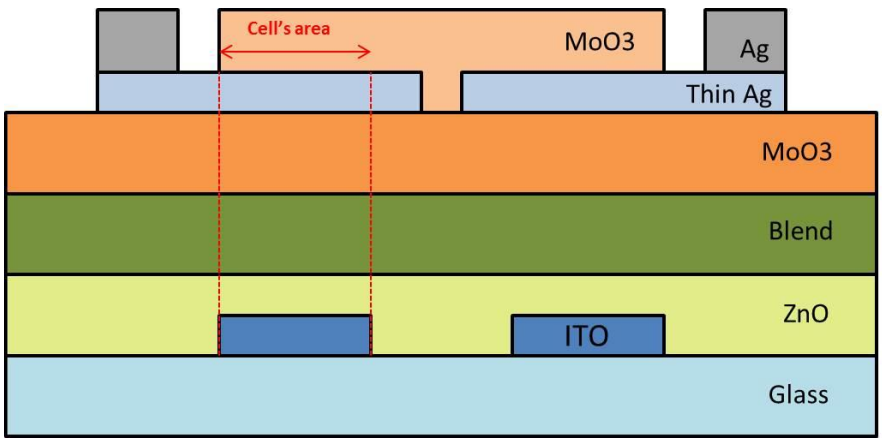

Figure 3.13. semi-transparent cell's layer structure in 2D. The layers are schematically shown in the previously described structure (thicknesses are not in scale). The cell area is the overlap between both electrodes. The MoO_3 protection for the Ag electrode is shown, as well as the thick Ag contacts placed outside the cell's area but still contacting the electrode.

3.2.6. Characterization

Even though many characterization measurements could be done to obtain different information about the cell characteristics, the basic ones I have been performing after finishing every batch have been:

- Current density-voltage (J-V) measurements: the finished device was fixed facing down, for the light to enter from above through the glass and the transparent ITO electrode, and was put under the AM 1.5G spectrum illumination from the solar simulator. The electrodes were contacted and plugged to the source-measurement unit, which was driven by the Tracer2 software and exposed the electrodes through a range of voltages between -0.5 V and 0.8 V, while measuring the obtained corresponding current. From these measurements, the software automatically obtained the J-V curve and calculated parameters like J_{sc}, V_{oc}, FF and PCE. The ITO electrode was contacted by a clamp and the back silver electrode was contacted by a gold tip. The measurement was performed in ambient atmosphere.
- External quantum efficiency (EQE) measurements: To verify the J_{SC} obtained with the J-V measurements, the EQE was measured with an EQE setup. It illuminates the substrate with a monochromatic beam and integrates the obtained current over the range of corresponding wavelengths at which it was measured. The setup has to be calibrated each time with a silicon calibration photodiode.
- Other measurements: at some points of the experiment, depending on experimental needs or performance mismatches, measurements like the UV-Vis spectrum transmission or an AFM surface characterization were also performed.

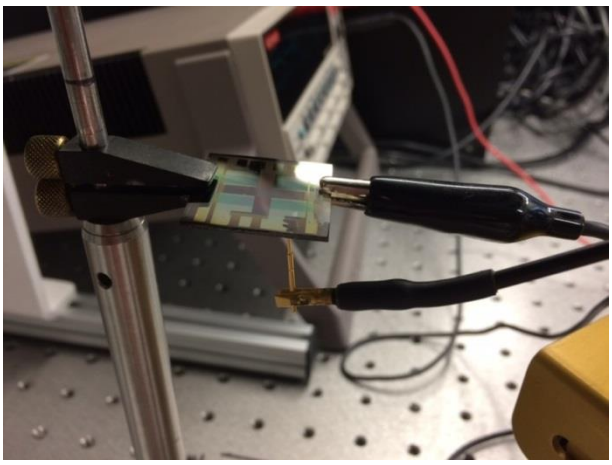

Figure 3.14. A typical J-V measurement setup (illumination was switched off to take the picture). The ITO stripes are contacted by the conductive clamp, and the silver back electrodes are contacted by the gold tip.

4. EXPERIMENTS, RESULTS AND DISCUSSION

In this fourth section, all the experiments and research activities that I performed during my 5-month stay at ICFO's Organic Nanostructured Photovoltaics group will be described. They will be listed chronologically, as most experiments' design was motivated by the results of previous ones.

When I first arrived in the group, I started fabricating opaque OPV devices. Besides from learning purposes, opaque devices were important for the project as opaque cells provide us a reference to quantize the losses in performance of semi-transparent ones. After setting that reference, I learned the fabrication process for semi-transparent cells and made a study of the up-scaling losses. In other words, I fabricated many semi-transparent devices of different areas and studied the performance against cell area dependence. Thanks to this information, a hypothetically improved device was designed, choosing an area for which losses would not be too high. The design included the addition of a silver grid in the electrodes for an enhanced charge collection and a decreased electrode series resistance. Following this ideal design, a study of the conductivity of silver was performed in order to infer which should be the thickness of the grid giving the best performance and avoiding visual appearance deterioration. This allowed us to set reasonable parameters for the new design's features. Next to this, we studied the viability of growing an OPV cell on top of a silver grid, as it was necessary to build the ideal new design. This verification was followed by the fabrication of large-area devices, which was not really successful, and had to be substituted by the actual study of the performance improvements expected for the addition of grids. In order to do so, a more realistic design was implemented to allow for a comparison between devices with and without the collecting grids. This was in fact the most important experiment, as it could demonstrate the utility of silver grids for up-scaling. The work flow during my thesis is shown in figure 4.1.

Figure 4.1. Scheme showing the subsequent experimental steps followed during the project.

4.1. Opaque OPV

In this first study typical opaque cells were built as references. Their back electrode thickness was of 100nm and their area was of 0.06 cm^2. They were characterized to obtain the J-V curves, cell parameters and quantum efficiencies. The results were stored for further comparisons with semi-transparent devices and can be visualized in figure 4.1 and table 4.1.

Device	Size (cm^2)	Jsc (mA/cm2)	Isc (mA)	Voc (mV)	FF (%)	Eta (%)
Opaque cell	0.06	17.15 (17.12)	1.03 (0.98)	801.1 (796.3)	72.7 (65.2)	9.16 (8.9)

Table 4.1. Results obtained from measuring 3 samples with 8 opaque cells each. Values in black show the best performance achieved, and green numbers are the average of the 24 tested cells.

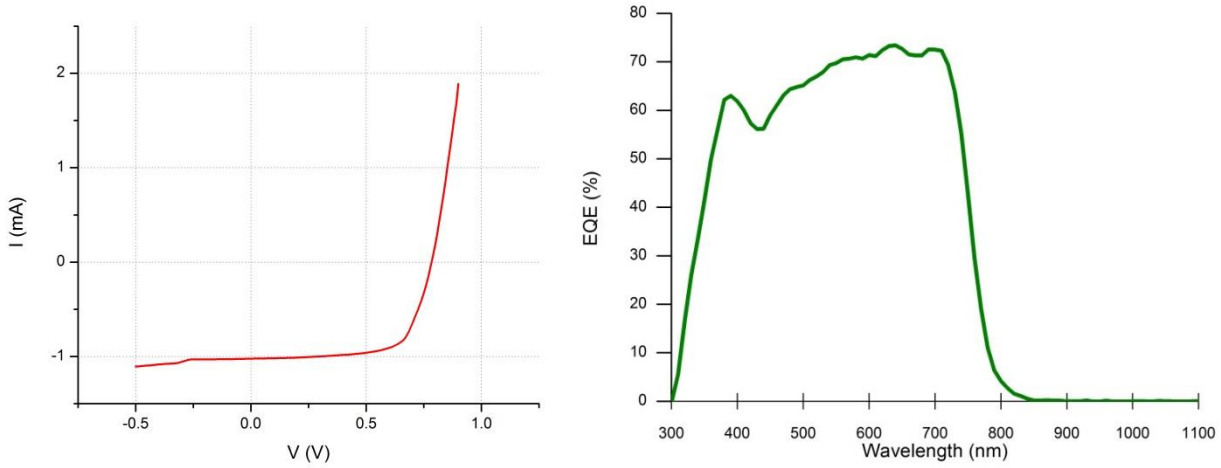

Figure 4.2. I-V curve (left) and EQE curve (right) of the best performing cell from the experiment.

4.2. Up-scaling losses of semi-transparent OPV devices

The aim of this experiment was to characterize and study how the performance in semi-transparent OPV decreases when increasing device area, while comparing their characteristics with opaque cells. To obtain a semi-transparent OPV it is required to thin down the back metal electrode layer in order to reach thicknesses where it is transparent. In most of the experiments we reduced such thickness to 10nm.

There's an obvious loss in efficiency as a consequence of reduced photocurrent given the lack of back electrode's internal reflection, but other kind of losses also appear within the devices. The principal experimental losses that have been found through up-scaling are the following:

- Correctly working device statistics: when building semi-transparent OPV devices, the metal layer is thinner and thus more susceptible to manipulation, impurities in between layers and damage. For large-area devices of this kind, as each cell covers a higher surface within the substrate, the probability of being damaged or having a short-circuit between electrodes due to an impurity in the substrate increases. Having a short-circuit in the cell leads to almost no voltage difference between electrodes and the device acts just like a series resistance.

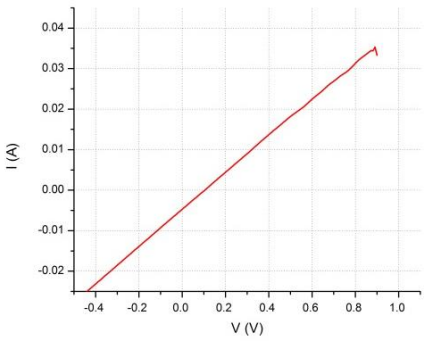

Figure 4.3. Short-circuit in an I-V measurement.

- Losses in Fill Factor: As the back electrode is thinner, its intrinsic conductivity is decreased. This fact is aggravated by the silver agglomerations that happen for thin layers, adding difficulties to current flow. These effects increase the electrode resistance and lead to FF losses, as the typical J-V curve loses its squareness, opposite to the ideal case. In other words, the maximum power point decreases.

The different devices were built using the standard masks owned by the Organic Nanostructured Photovoltaics group in ICFO. In Figure 4.4(a), it is shown the stripe pattern for the ITO electrode. Figure 4.4(b) shows the masks for the silver in the case of the small cells of 0.06 cm^2. The cells are formed in the intersection of the ITO and Ag rectangles, as indicated in red in Figure 4.5. Similarly, using other masks together with the ITO stripes, samples of 0.18 cm^2 and 0.45 cm^2 are fabricated.

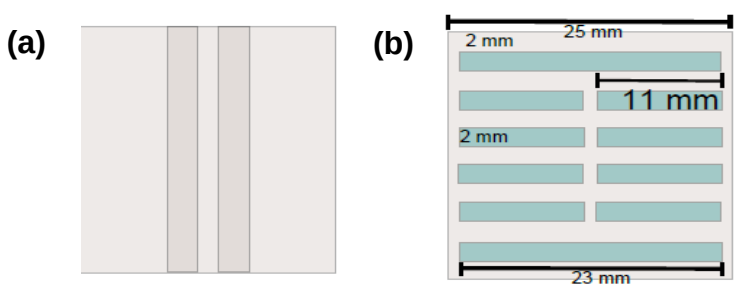

Figure 4.4. (a) ITO pattern in the utilized substrates. **(b)** Mask for the metal electrode used to produce the small samples of 0.06 cm^2

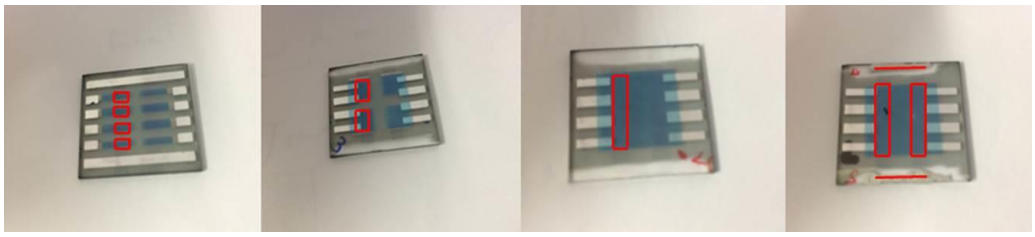

0.06cm^2 **0.18cm^2** **0.45cm^2** **0.9cm^2**

Figure 4.5. Built devices with different areas. The cell's area (two electrodes intersection) is shown for each case (red rectangles). In the 0.9 cm^2 device, the ITO stripes were short-circuited with a highly-conductive silver paste to acquire a cell adding the area of the two sub-cells. Cells are contacted in the thick silver right-left stripes for the back electrode, and in the top-bottom cleaned layers for the ITO front electrode.

The plot obtained by these two first studies features the FF and PCE of each device in terms of its area, as well as the opaque reference in a flat line to allow for a visual comparison.

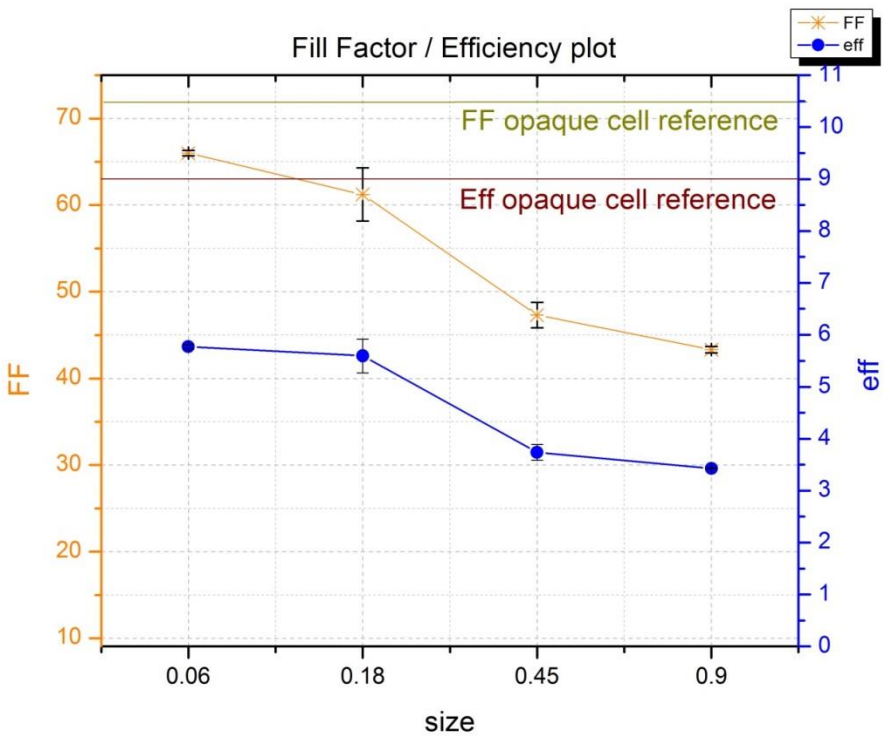

Figure 4.6. Up-scaling of the built semi-transparent OPV cells. Blue plot shows the PCE (%) and orange plot shows the FF (%). Horizontal red and green lines show the opaque reference's performance in PCE and FF, obtained in the previous section. Sizes are in square centimetres (standard units for PV).

For the implemented designs, the charge carriers have to travel increasing distances in the electrodes for larger areas. In this design this is particularly happening for the ITO stripes, as they can only be contacted in the top and bottom cleaned parts, and thus charges have to travel all along the ITO stripes before being collected. This is one of the reasons why, for example, there aren't almost any losses in FF when increasing the area from 0.45 cm^2 to 0.9 cm^2: as the

two stripes have been contacted with silver paste to increase the area, without increasing the length that charges have to travel, charge collection has not been deteriorated and thus, losses don't appear. The fact that ITO's electrode length is the determining parameter for this experiment suggests us to make a plot showing the electrode travel distance dependency instead of the area. This is shown in figure 4.7.

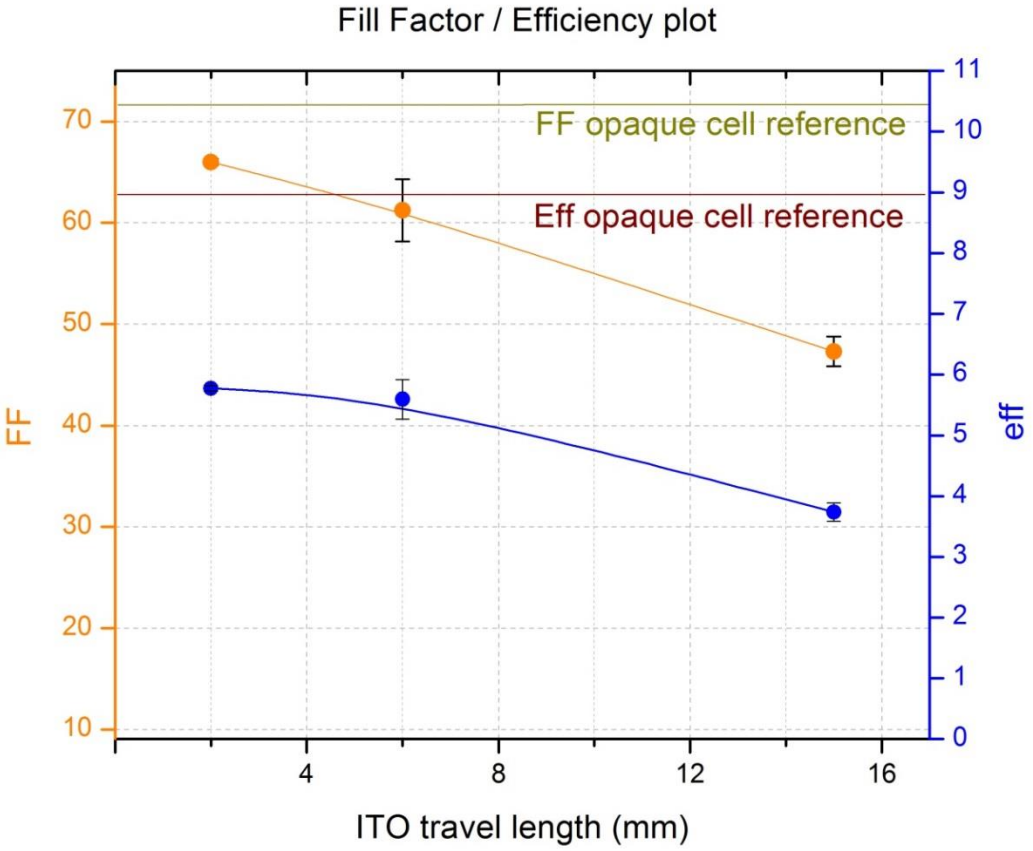

Figure 4.7. Up-scaling dependence in terms of the distance charge carriers have to travel through the ITO. The distance travelled through the silver electrode has been neglected as it is barely varying between samples in comparison with ITO electrode. In this plot there are 3 sample points instead of 4, as the samples of 0.45 cm^2 and 0.9 cm^2 have the same ITO travel length due to the fact that the ITO stripes have been contacted to increase the area.

From this study, we were able to visualize that there are significant losses when increasing cell's area, as the theoretical expectations predict. It also allowed us to realize about the experimental difficulties of the up-scaling. As a conclusion of the study, we saw that FF can be maintained above 60% for electrode travel distances up to 6mm. This information will be used in the subsequent steps to design large-area devices with reasonable electrode travel distances.

We finally characterized the built devices in order to quantize their transparency, and compare its effects on cell performance with the opaque cells.

Figure 4.8 shows the transmission curve of the semi-transparent cells for the UV and visible wavelength range. Even if it was measured for just one of the samples, it can account for all of the cells from this experiment, as they were all built in the same batch, thus in the same conditions.

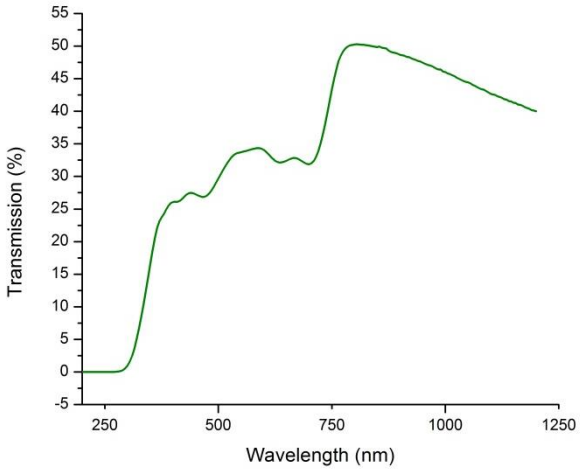

Figure 4.8. Percentage of transmission of incident light for each wavelength in the UV-Visible spectrum, measured for a 0.06 cm^2 sample.

Figure 4.9 features the EQE curves from an opaque reference of the previous section and a semi-transparent cell from the current section.

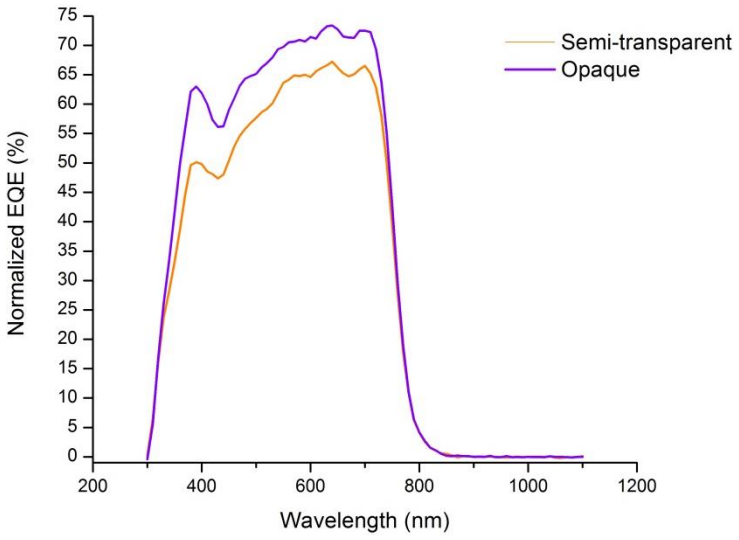

Figure 4.9. EQE curves from an opaque reference (purple line) and a semi-transparent device (orange line). Both cells have an area of 0.06 cm^2.

It is clearly shown how opaque cells have an increased EQE for all wavelengths. This is due to the increased internal reflection of the thick silver electrode, which reflects in all of the tested wavelengths.

4.3. Ideal design to maximize cell's area

After the previous step, an ideal semi-transparent OPV, performance-improved device was designed. It was used as a clarifying image showcasing the objective we wanted to achieve and was presented on group meetings as a motivation for the experiments that we were carrying out. It is shown in figure 4.10.

The design represents a substrate (blue box) with two wide ITO stripes (black rectangles) for a large area device: each stripe has 2 cm^2. All the cell's layers including the silver back electrode are represented by the yellow box. The blue lines represent thick layers of Ag in grid-like patterns. There are grid lines contacting the ITO electrodes and contacting the silver electrode (top of the yellow box) to collect charges before they travel long distances through the electrodes. These charges should travel through the electrode until they reach the closest grid line, as its increased thickness in comparison with the electrodes yields a decreased resistance, lowering also the device's overall series resistance. Using the information obtained from the previous study, grid lines are designed not to let charges travel more distance than **6 mm** through the electrode. This way, ideally, the FF would be **above 60%** for a 2 cm^2 cell. The grid lines from both electrodes are made to coincide as much as possible to reduce opaqueness and interfere as little as possible in the visual appearance of what's behind the cell. Each grid has one contact (little blue rectangle). As there are two ITO stripes, there are two different overlaps between ITO and the top silver layer, and thus two cells. However, the grid contacts both cells' front and back electrodes, creating a two-cell module by connecting them in parallel.

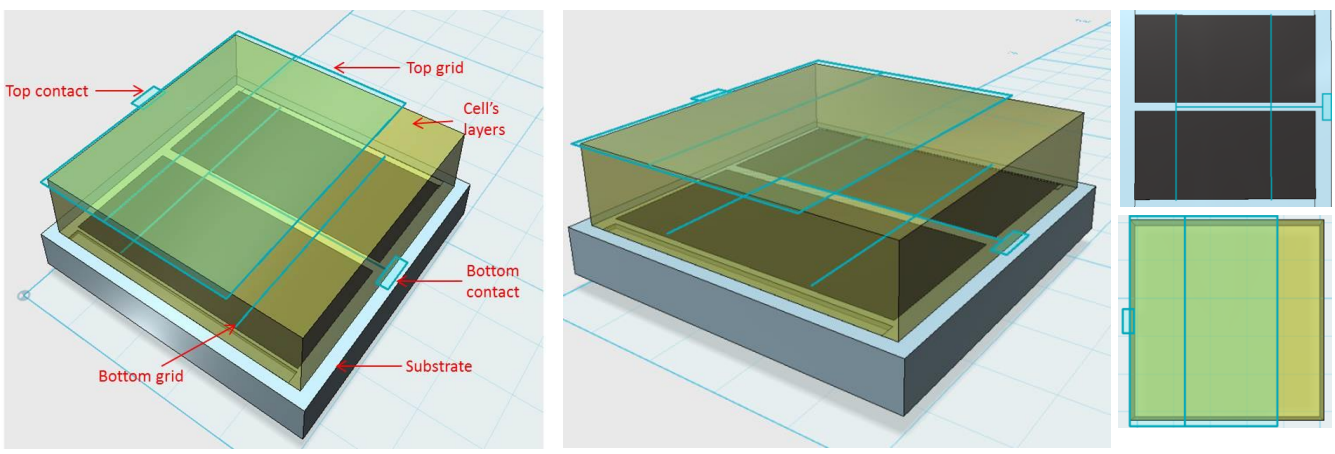

Figure 4.10. Different views of the hypothetical final device. Designs made with the use of the program *123D Design*.

To be able to produce devices following this design while having improved performance, it is basic to make three studies:

1) Study the conductivity (or equivalently, resistivity) of Ag to be able to set the proper grid's thickness to ensure the desired resistance enhancements are achieved.
2) Prove if it is possible to grow cells on top of a thick grid layer.
3) Compare devices of the same area with/without collecting grids to see if the theoretical improvements in FF are achieved.

4.4. Resistivity of Ag in terms of layer thickness

After setting the objective of enhancing the electrode's conductivity by contacting it with a silver grid, silver layer's resistivity (inverse of conductivity) has to be characterized. There are three basic motors motivating the making of this experiment:

- Study and prove the creation of silver islands for thin layers:
  When depositing thin Ag layers, particles tend to interact with each other and form agglomerations (even when cooling to reduce interactions). This phenomenon increases the resistivity of the layer by promoting non-homogeneity, and has been previously characterized through atomic force microscopy imaging to spot the silver "islands" and measure their size. However, one of the aims of this study is to set a threshold in the layer's thickness for which islands start to create (for the lab's particular setup properties).
- Set a bulk resistivity for silver layers:
  For thick Ag layers, resistivity is expected to be a constant value. This looks like a reasonable expectation, because when the layer is thick enough for the "islands" to contact with each other, the resistivity ends up being an intrinsic property of silver, and not a geometrically dependent parameter. Through this experiment, we would like to obtain this value, as it is the minimum resistivity we can obtain with silver layers.
- Set a bulk/thin layer resistivity ratio to design the grid properly:
  The Ag back electrode's layer thickness is fixed at 10 nm for transparency purposes, and for this thickness its conductivity is not as good as ITO. Keeping in mind the fact that the Ag bulk resistivity (and so grid's resistivity) cannot be improved, the relation between our thin and thick Ag layer's resistivities will be a constant value that we cannot change. The aim is to obtain that value, which will allow us to set which has to be our grid width, for it to yield an improvement in resistance in comparison with the thin electrode.

The way in which this experiment was carried out is by making silver depositions of different thicknesses on flat, non ITO covered glass substrates and inferring the layer resistivity for each one. Different glass substrates were covered with 5 nm, 10 nm, 20 nm, 25 nm, 35 nm, 40 nm, 80 nm and 150 nm of silver respectively, without using any shadow mask. Then they were exposed to increasing voltages and the produced current was measured. The resulting I-V curve was a resistor-like straight line, and its slope gave the resistance of each silver layer. By knowing the geometrical parameters of the layers (thickness and substrate size) and their resistance, the resistivity of each layer was calculated using the resistance definition (formula 6).

$$R = \frac{\rho \cdot L}{A} \qquad (6)$$

R is the resistance, ρ is the resistivity, L is the length of the object and A is the area of the object transversal section, that is, charges have to fit a section A to travel a length L in an object of volume V=L·A.

The expectations for the resistivity-thickness curve were to obtain a decreasing resistivity for increasing thicknesses, as islands will get bigger and closer to each other, increasing this way the current propagation through agglomerations. But this decreasing tendency was also expected to get smoothened and finally stopped by the contact of all the growing-islands for a determinate thickness, from which thicker layers will not decrease the resistivity anymore. Surprisingly, our results differed considerably from these expectations. They can be seen in figure 4.11.

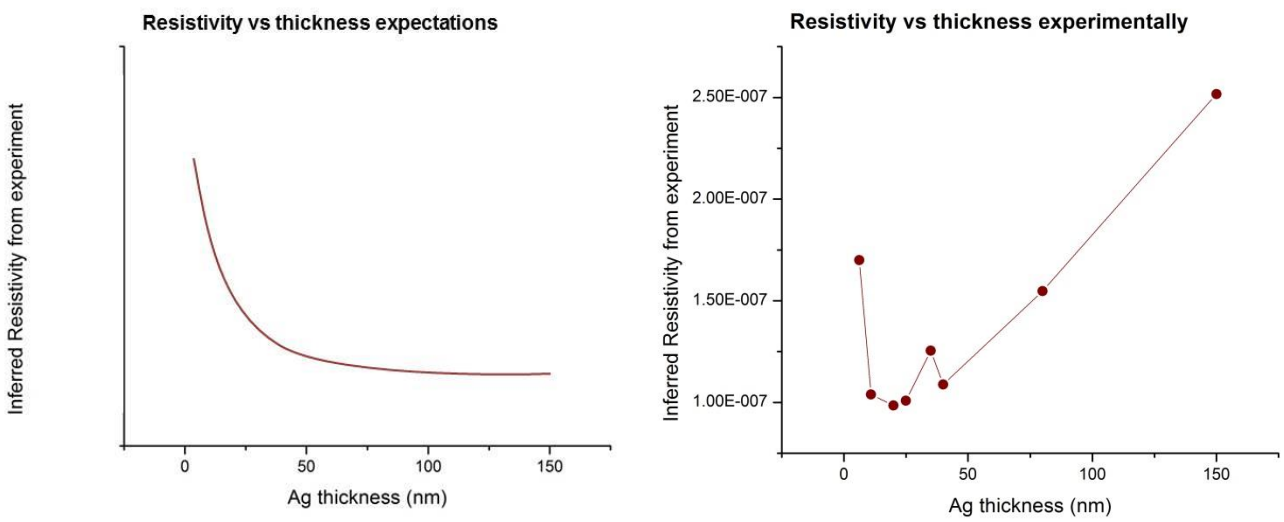

Figure 4.11. Recreated resistivity in terms of Ag thickness curve showing our expectations (left graph), and experimental curve obtained with the described method. Resistivity's units are ohms per meter (Ω·m).

As the results did not fit the expectations, but did not follow any logical relation, we concluded that we had to be mistaken in the way to infer the resistivity. That was true, because silver layers cannot be modelled as cubes, even less when they are thin and have big agglomerations or “islands”. One proof of this is shown in figure 4.12. We realized about this fact when we characterized the silver’s surface of a 10 nm layer in the AFM Microscopy, and saw the big proportions of such agglomerations.

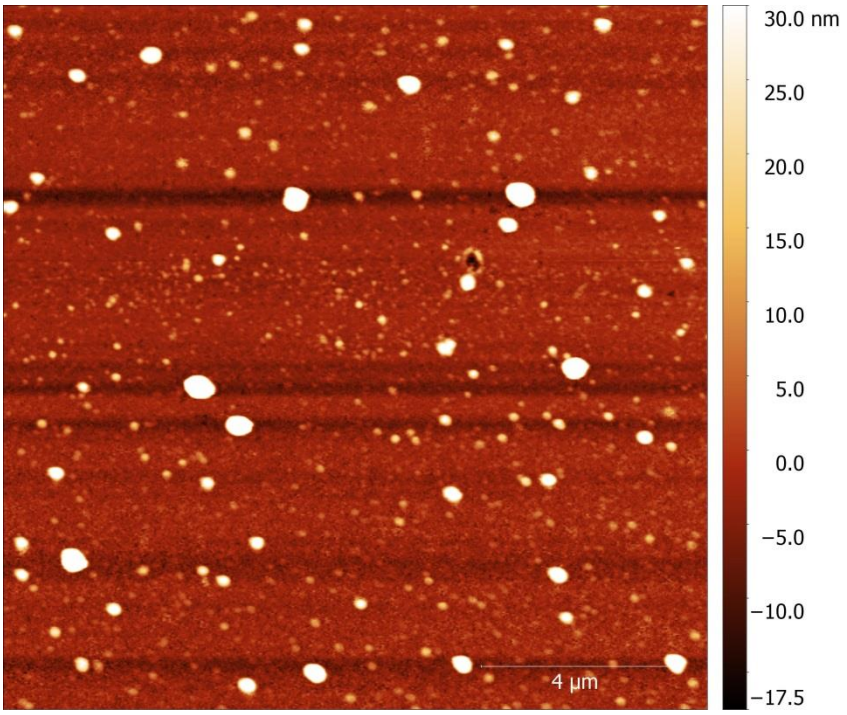

Figure 4.12. AFM (Atomic Force Microscopy) image of the top silver surface of a glass substrate covered with 10 nm of silver. The z-axis color scale is shown in the right. The white spots are the Ag “islands”. The image gives an idea of the average size of these agglomerations, as they are white (30 nm height approximately) while the background is mainly red (0 nm approximately). This gives a guidance height for agglomerations of around 30 nm, for silver layers that are expected to be 10 nm thick.

As a solution to obtain the actual layer’s resistivity for the experiment, a four-point measurement was used. Apart from the advantages in accuracy that this method provides, it proportions directly the value of the resistivity of the sample, without having to infer it by obtaining the resistance and modelling the layer’s geometrical characteristics.

After measuring the samples, the expected curve was obtained. It is shown in figure 4.13.

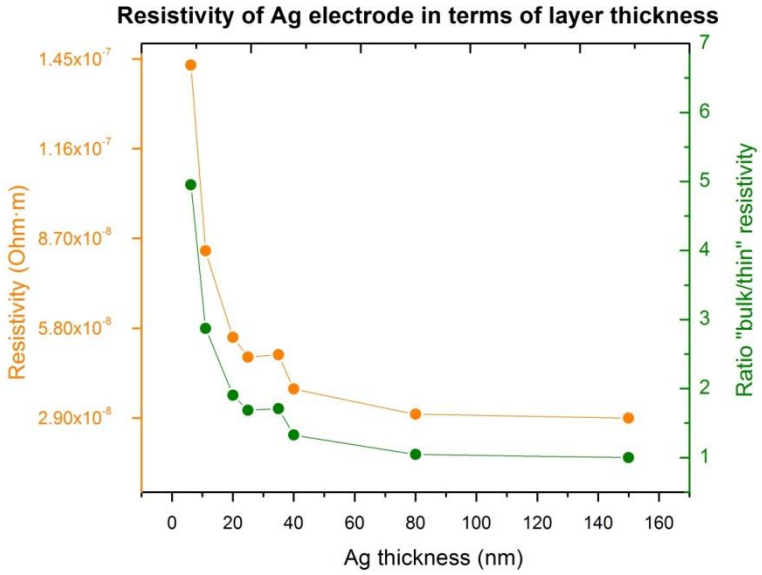

Figure 4.13. Thickness dependence of resistivity in Ag layers. Orange plot shows the resistivity in ohms per meter (Ω·m) in terms of the thickness in nanometers (nm). Green plot represents the ratio between the actual layer's resistivity and the bulk resistivity (or the constant resistivity value for thick layers). Even if we call it bulk/thin ratio, it is calculated by dividing the thin layer's resistivity by the bulk one.

As we can see in the plot, the resistivity decreases and finally tends to a constant value, for increasing thicknesses. Adding this information with the AFM image, we can confirm the existence of silver agglomerations for thin layers. Not only we can confirm it, but also set a thickness threshold for which those agglomerations will not yield any consequence on the layer's electrical behaviour. This threshold can be directly extracted from the graph, and it is of around **70-80 nm.** From that point, depositing thicker layers will not reduce the resistivity anymore. This lowest value for the resistivity, or just silver bulk resistivity is of **$2.9 \cdot 10^{-8}$ Ω·m**.

Finally, as the last conclusion of the experiment, we have obtained a thin/bulk layer ratio, for the 10 nm layer, of 3. In other words: the 10 nm thin layer's resistivity is 3 times larger than the bulk resistivity.

Using this bulk/thin layer ratio for 10nm layers, imposing a grid's layer thickness of 150 nm (standard bulk thickness in our group), and imposing a final thin/bulk layer resistance ratio of 5, the only parameter left to determine is the grid's width. We decided to impose a thin/bulk resistance ratio of 5 to ensure a significant resistance reduction is achieved by the grid, and thus, charges will travel through it rather than the semi-transparent electrode. By finally isolating the grid's width, it is obtained a value of **200µm**.

Thanks to this study, we obtained a guidance value for the width that the grid should have in the desired design, in order to enhance charge collection by effectively reducing the semi-transparent electrode's resistance.

4.5. OPV cells on top of a thick silver grid

The following experiment was done in order to prove the possibility to build OPV cell's layers on top of a thick silver grid. It is not trivial to speculate whether it is possible, as the depositions could lose homogeneity because of the non-flat substrate creating a non-ideal behaviour in the cell or even causing a short-circuit. This is schematically simulated in figure 4.14.

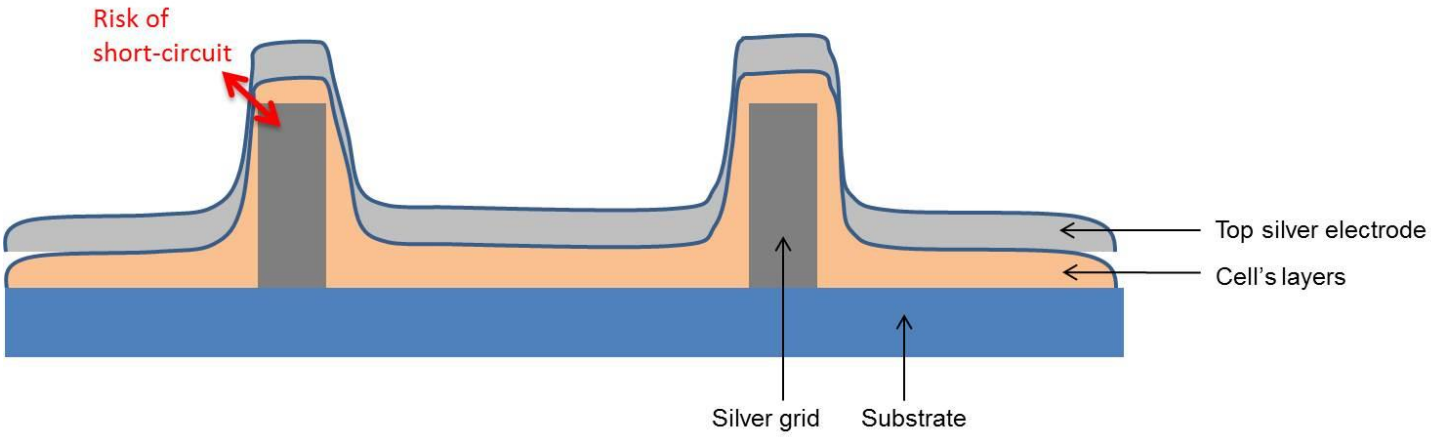

Figure 4.14. Illustration showing the main expected problem when depositing the cell's layers on top of a thick layer of silver. The grids are shown transversally in this 2-dimensional section of the device, deposited on top of a glass and ITO substrate, and under the cell's layers and back electrode. The layers are expected to acquire a thinner shape in the vertical walls of the grid, increasing the possibility of creating a short-circuit between the bottom grid (which contacts the ITO front electrode) and the silver from the back electrode.

To start the experiment, one step had to be added in the fabrication process: depositing a thick silver grid contacting the ITO, right after the cleaning process and before the deposition of the ZnO layer. The grid's thickness was chosen to be of 150nm, and it was deposited using the evaporator, at a rate of 1 Å/s, using a grid-like shadow mask of 200 µm thick lines. After this layer, all the subsequent ones were deposited, following an opaque cell process. This was due to the fact opaque cells' process takes a shorter time and does not alter the experiment's results: if it is not possible to create a functional cell on top of a grid, our sample won't work either on a semi-transparent cell or in an opaque one.

The results were positive, as both cells were proved functional (see table 4.2 for cell's comparison through more specific parameters).

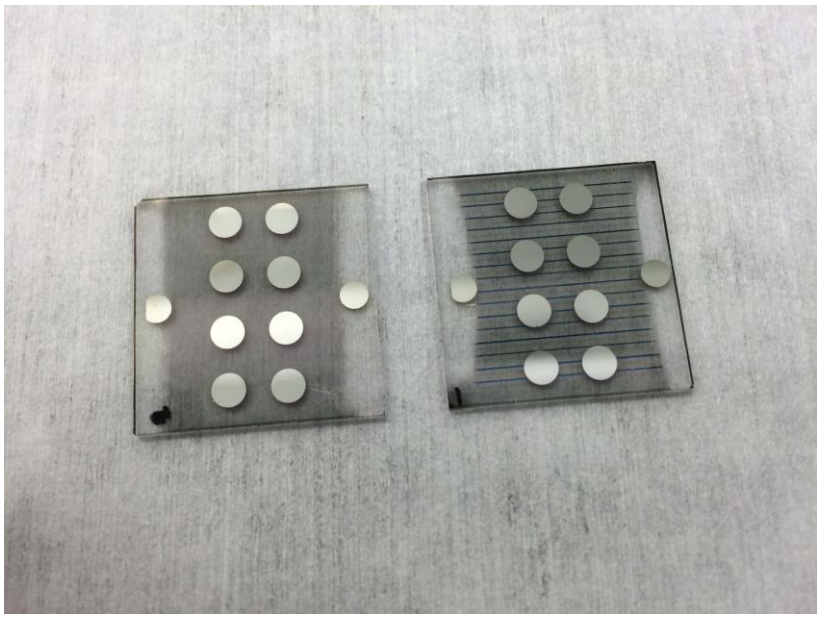

Figure 4.15. Picture of the two compared samples: no grid sample (left) and bottom grid sample (right).

As it can be seen in table 4.2, the device having the grid did not show enhanced behaviour. This does not contradict our initial expectations, as they were made for semi-transparent devices. In opaque cells this difference should be negligible, as their FF is already very high.

	Jsc average	**Voc average**	**FF average**	**Efficiency average**
Grid	13.65 mA	795.54 mV	70.04	7.6
No grid	14.67 mA	790.60 mV	69.17	8.02
Grid / Nogrid	93.06%	100.62%	101.25%	94.79%

Table 4.2. Performance averages of the opaque cells without bottom grid, the opaque cells with grid, and ratio between their performance parameters. It is clearly shown that the grid does not alter the performance for this opaque configuration.

Finally, as a conclusion, we can affirm it is possible to grow cells on top of a 150 nm thick grid.

4.6. Large area semi-transparent OPV

After the previous findings and demonstrations, we started fabricating large area devices. The aim was to try to see some improvements by introducing grids on top or/and bottom of such large area devices, and compare with non-gridded references. The experiment was done using masks already purchased from the group, to try to demonstrate the utility of the grid and posteriorly design an optimized device and purchase some custom masks for it. The cell's areas were of 1.2 cm^2 and 2.25 cm^2, as the biggest masks that the group has allow for this size.

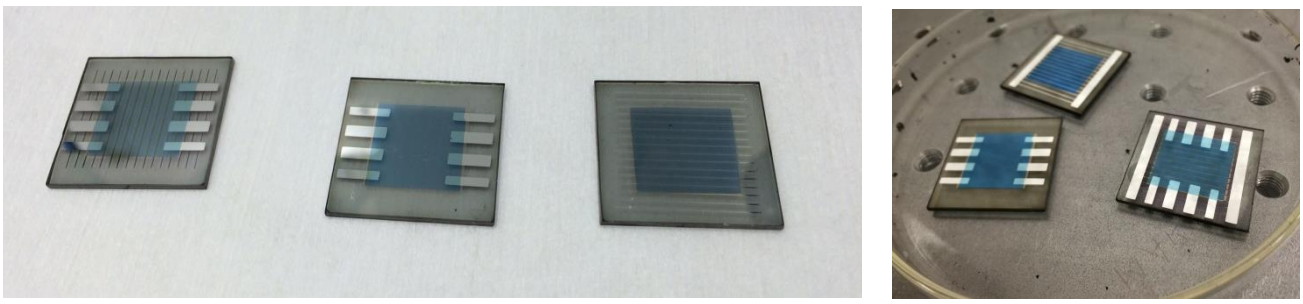

Figure 4.16. Two different batches of 2.25 cm^2 semi-transparent OPV devices. Some of the samples have a 200 μm grid in the front or in the back electrode, and some don't have it to work as references.

To be able to produce such large size cells, substrates with 2-stripe ITO pattern could not be used, because the stripes' area is too small (remember that the ITO's and thin silver electrode's overlap defines the cell's area). Instead, we used full ITO-covered substrates, and produced one large area cell per substrate. Using these new substrates added one more step in the fabrication process, before the substrate cleaning: etching of the ITO layer. As previously stated, for the semi-transparent cells, it is not recommended to directly contact the back electrode with the gold tip, as it could be harmed due to its low layer thickness. To contact it, a thick silver contact layer is deposited out of the cell's area but still contacting the thin silver. In a substrate fully covered of ITO, there would be overlap between electrodes, and this thick contact would produce a small opaque cell that would alter the results of the experiment. Cleaning the blend before depositing the contact to avoid the creation of an opaque cell is also altering the experiment, as the ITO of the substrate would be contacting the thick silver, and so both electrodes would be in short-circuit. The way to solve this problem was by covering most of the cell with tape, and then performing an etching process for the ITO in the non-protected surface. This way, we obtained a substrate without ITO covering in one side, where we would deposit the silver contacts for the back electrode.

Unfortunately, when measuring the large area substrates, the majority were short-circuited or working badly. This happened due to the fact that any impurity being in the substrate was affecting and short-circuiting the cell. In previous smaller area cells, that impurity would have maybe broken 1 out of 8 cells, but in a substrate covered by just one big cell, the impurity affected the whole device. However, I was able to get two well working reference devices (without grid) of 1.2 cm^2 and an ITO charge traveling distance of 18 mm, that were used as an addition of one more point in the up-scaling losses curve.

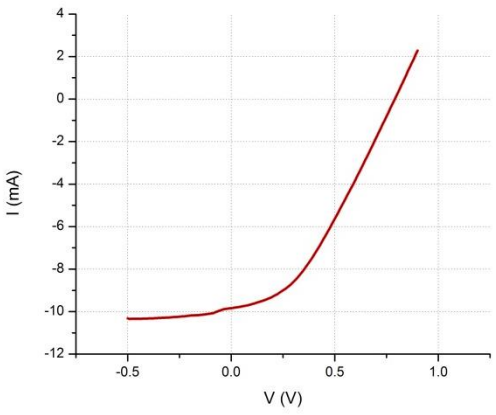

Figure 4.17. I-V curve of one of the operative large area devices, measured under solar spectrum simulation.

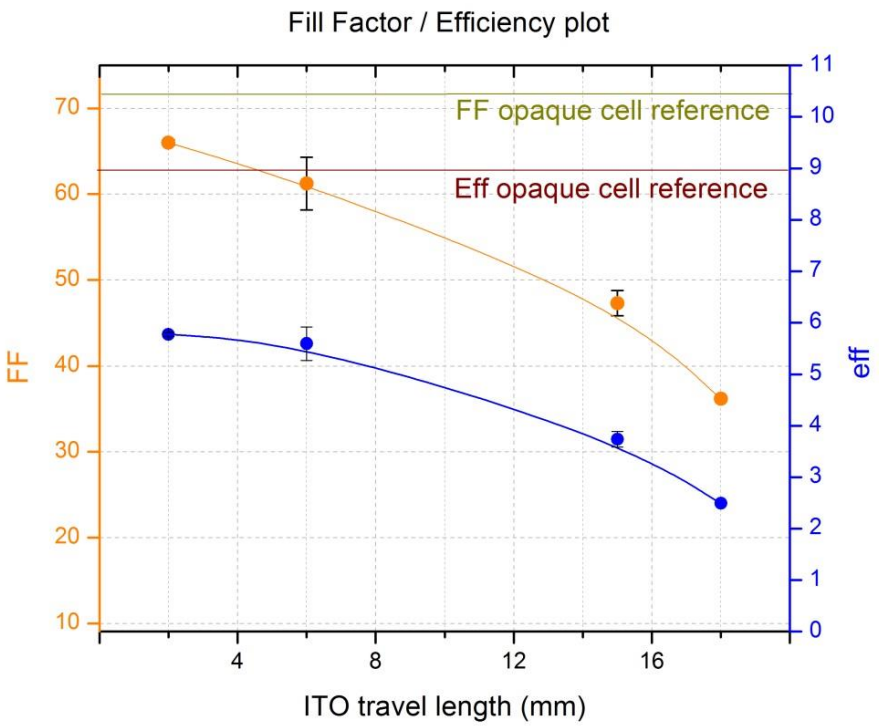

Figure 4.18. Semi-transparent OPV devices' up-scaling losses. The graph is exactly the same as the one in figure 4.5, but with the addition of the sample with the largest ITO travel length (point corresponding to 18mm).

4.7. New grid design

As a next step in the project, we realized that working with such large-area devices was difficult or nearly impossible, because the fabrication process was really long and only a small proportion of the samples were operative.

In order to prove whether the grid can enhance the performance or not, I created a new device design, with smaller size cells of 0.18 cm^2, especially made for the desired experiment. This new design allowed for the placing of 4 cells per each substrate, thus increasing the probabilities of obtaining a functional cell in each sample. It also allowed for the utilization of the standard ITO 2-striped substrates, which saved time because no etching was then needed. The main purposes of the design, in terms of expected results, were:

- Enhance charge collection by placing only one grid line, to disturb transparency as little as possible.
- Collect the charges in two different places for each electrode: at one side of the cell and in the middle of it by the grid line, thus reducing the charge travel distance through electrodes to the one in 0.09 cm^2 cells (half the area of the new design).
- Be able to control the cell's area precisely by setting illumination masks while measuring. Illumination masks were designed to cover from light those zones where thick silver is put to contact the back electrode with overlap with the ITO, thus creating an opaque cell and slightly changing the device's parameters.
- Obtain the same performance as in cells with half of the new design's area.

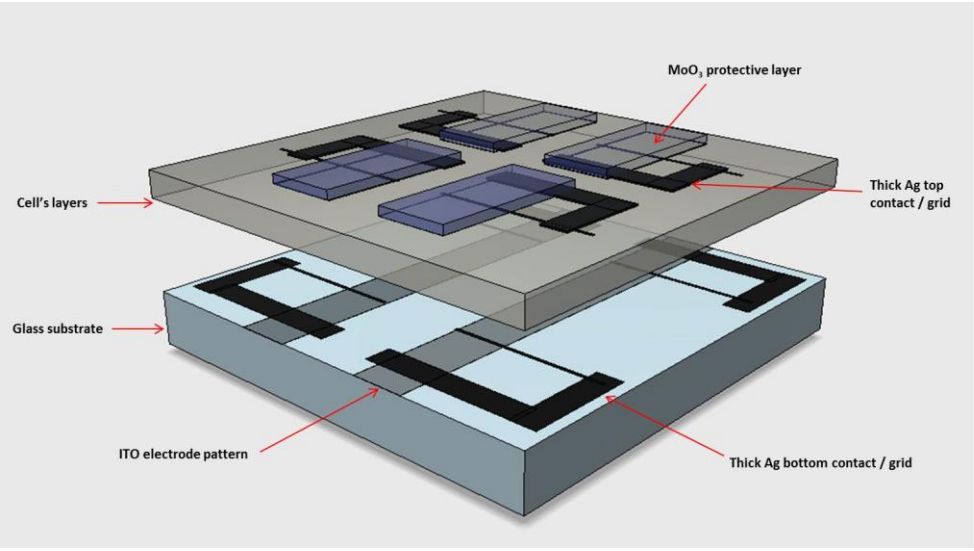

Figure 4.19. 3-dimensional design of the new devices. The substrate with ITO, silver contacts and grids is separated from the cells' layers, top contacts and MoO_3 protective layers to facilitate visual understanding.

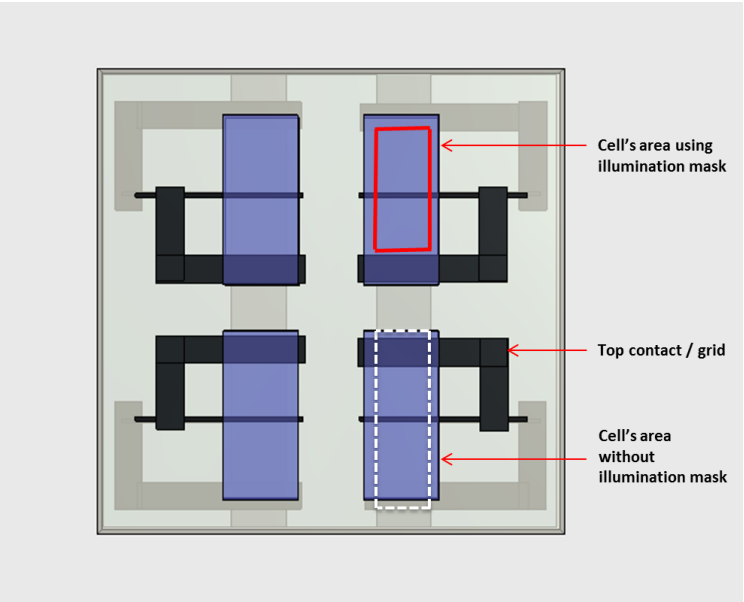

Figure 4.20. Top view of the 3D design of the new device. The white rectangle represents the whole cell's area, combining opaque zones (where there is overlap with the contacts and grid lines), and semi-transparent zones. The red rectangle shows the only illuminated area when placing the illumination mask so that the size gets reduced to 0.18 cm^2.

The masks had to be designed taking into account manufacturer's precision, desired layer overlaps and the different steps of OPV fabrication. They were purchased and fabricated outside from ICFO, and I had to wait for one week to receive them and start the experiment.

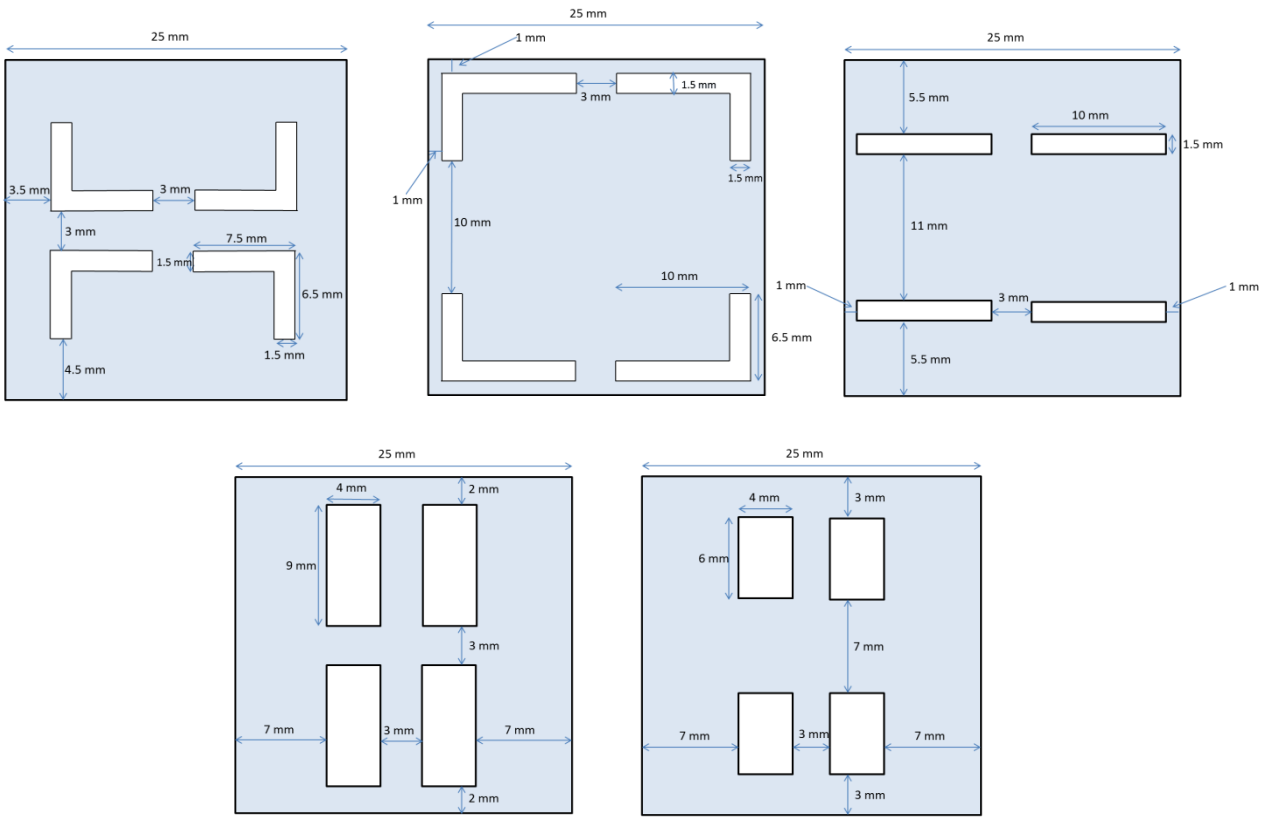

Figure 4.21. Mask designs that I sent to purchase in order to create the new device. The three top masks are made for thick silver depositions for the contacts and grids (the one in the right has to be combined with a full grid mask to only let 4 lines be deposited). The bottom-left mask is made for the EBL and thin electrode, and the bottom-right one is the illumination mask.

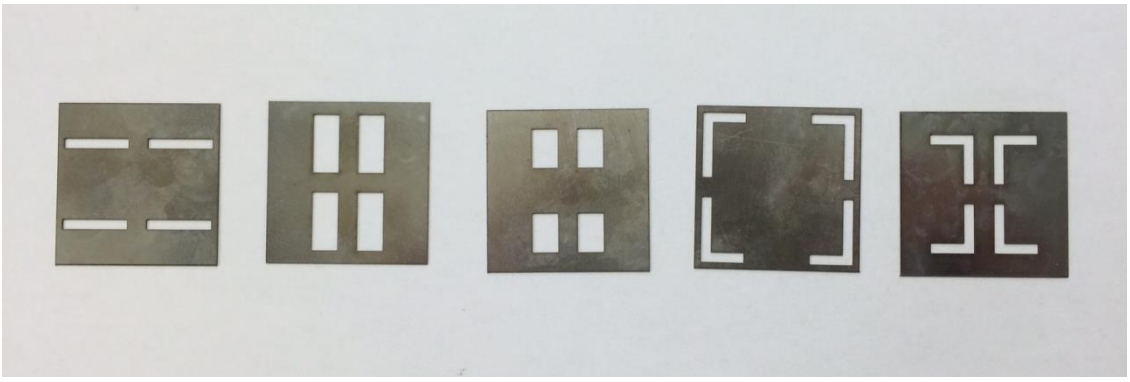

Figure 4.22. The designed masks after receiving them at ICFO.

The fabrication process was longer for these devices. After the cleaning routine, the thick silver ITO contact and its associated grid lines had to be included through two Ag vapour depositions (see figure 4.23), followed by the usual coating of the HBL and the blend. From this point on, I started using the **degradation-improved method** because of group requirements. After the spin-coatings of the ZnO, PFN and blend, the vapour deposition was carried out for the thin MoO_3 and thin silver layers. At this point, the thick silver top contact and grid lines were put through two vapour depositions, and followed by the protective thick MoO_3. Summing up, three thick silver depositions were added, increasing 2-3 hours the fabrication process duration.

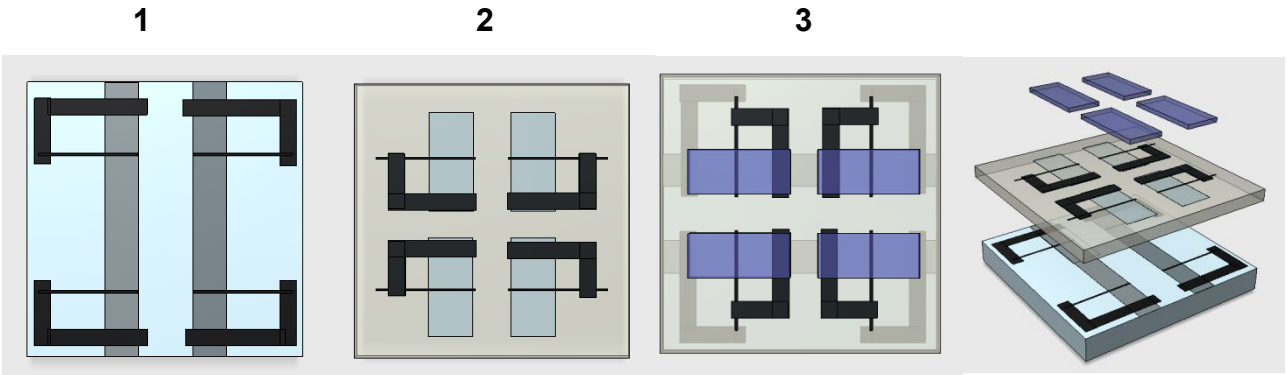

Figure 4.23. View (1): ITO's silver contacts and grid lines (black figures). View (2): ZnO, PFN, blend layers (gray background), MoO_3 and thin Ag layers (blue rectangles), and top silver contacts and grid lines. View (3): finalized process with the protective, transparent MmO_3 layer (blue rectangles).

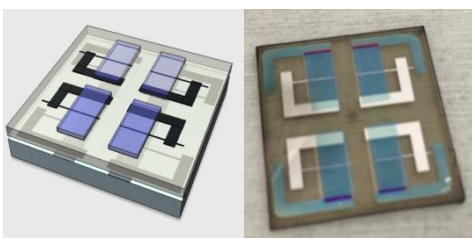

Figure 4.24. Pictures of 3D design (left) and real finished device (right).

First of all, before starting with the grid's experiment, a simpler and shorter one was performed in order to prove the new design was functional and avoid making wrong conclusions about the grid. I built two opaque (50 nm of Ag) new devices without depositing any grid lines, just the cell top and bottom contacts, and also built two opaque reference cells to compare. These references were built using older masks that had already been proved functional, and had an area of 0.18 cm^2. As the aim of the experiment was to count how many functional cells we could obtain with the new design, no illumination masks were used in order to simplify the experiment, and so the new design cell had an area of 2.25 cm^2. The area was similar enough to the references to compare their functional device statistics.

The results were:

- References: 4 out of 8 working
- My design: 1 out of 8 working

Device	**Size**	**J_{sc}**	**I_{sc}**	**V_{oc}**	**FF**	**Eta**
	[cm^2]	[mA/cm^2]	[mA]	[mV]	[%]	[%]
Reference	0.18	15.44	2.77	809.29	60.14	7.51
My design	0.255	15.54	3.96	797.41	63.43	7.86

Table 4.3. Table comparing the devices showing the best performance for each of the tested cells: my design and the reference.

A small proportion of the new design cells were working. Through inspecting closely, we reached the conclusion that it was due to a contact problem while measuring, as the measurement setup that we had in the lab was designed for the standard cells. Another possible problem could be the increased amount of required depositions, which can be harmful due to the increased manipulation of the substrates. One different argument to believe it was a contact problem was the fact that the only functional new design cell was performing better than any of the references.

Thanks to this pre-experiment, I performed the next study being really careful when manipulating the substrates, and thought about different ways to measure that could avoid bad contacts.

In the next experiment, I built three different kinds of semi-transparent devices (using two substrates per each): some 0.18 cm^2 new design cells, some 0.18 cm^2 references without grid,

and some 0.09 cm^2 references. These last ones were built in order to see if the grid cells could perform as well as them, while doubling their area.

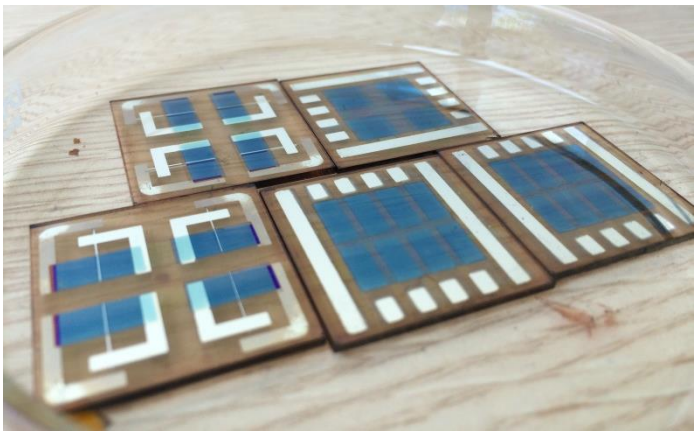

Figure 4.25. Picture of some of the built devices.

Device	Size	J_{sc}	V_{oc}	FF	Eta
	[cm^2]	[mA/cm^2]	[mV]	[%]	[%]
Grid cells	0.18	12.81 (12.67)	772.92 (777.29)	61.72 (60.47)	6.11 (5.95)
0.18 ref	0.18	13.96 (13.71)	774.65 (771.92)	61.17 (53.16)	6.61 (5.63)
0.09 ref	0.09	12.36 (12.51)	777.18 (776.36)	63.46 (59.78)	6.09 (5.80)

Table 4.4. Table with the best results and averages (green values between brackets) for each kind of cell.

The proportions of correctly working devices were: 4 out of 4 in the 0.18 cm^2 reference, 14 out of 16 in the 0.09 cm^2 reference, and 2 out of 8 in the grid new design cells. Even these proportions were still low for the grid cells, the conclusions one can extract from these results are that the thick silver grid is working correctly and the values are coherent with the expectations. It is possible to appreciate how the 0.09 references have a higher FF, in average, than the 0.18 references. But the most interesting comparison is the one between 0.09 cells and grid cells: in average, the grid cells overtake the FF losses coming from the increase in area (shown by the 0.18 references), and equal the 0.09 cells performance. Other coherent facts can be noticed: comparing the grid cells with the big reference cells it is possible to see how there is a decrease in the J_{sc}, which is partially influenced by the opaqueness of the grid, which covers a small amount of the whole illumination that the cell receives, with respect to its area.

Even though the results show the grid is really helping to up-scale without any loss in Fill Factor, the proportions are still not high enough to consider them definitely concluding. Further studies, with a bigger amount of masks to produce more samples per batch and an optimized measuring set-up for the specific design, could offer a definitive answer. However, the results are promising as the two working grid samples had a performance as good as the references with half of their area, contradicting the previously obtained up-scaling graphic, which in fact was their objective.

5. CONCLUSIONS

The making of this project and all its experiments has led to several concluding statements:

- Up-scaling losses:
  We have been able to quantize the Fill Factor and Power Conversion Efficiency losses when increasing the semi-transparent cells area, confirming the actual difficulties of up-scaling. We have particularized such information by studying the charge travelling length through ITO electrode dependence of cell performance, reaching the conclusion that 6mm of ITO is the maximum length for which charges can travel before being collected while reaching a device FF above 60%.

- Thin Ag layers:
  The study of thin silver layers has allowed us to reach important information about the semi-transparent back electrode and its conductivity. We have proved the expected creation of agglomerations of metal particles, and characterized their implications in terms of conductivity losses in the electrode. We have set a threshold in Ag layer thickness, from which thicker layers will not increase the bulk conductivity, of 80 nm. The silver bulk resistivity value for such layers has also been found, obtaining a value of $2.9 \cdot 10^{-8}$ Ω·m.

- Thick Ag grids:
  Finally, the previous studies have allowed for the design of appropriate devices to test the use of charge collecting grids. We have been able to prove the functionality of devices built on top of thick Ag grid lines, and to study and compare the performance of OPV cells of large area including and not including collection grids. The results have led to optimistic conclusions, as we have produced large devices doubling references area while equalling them in performance, through the addition of such grid lines.

As an outlook of such facts, further studies having the possibility of building larger amounts of cells with grids and optimizing the design for minimum experimental failure of devices, could determine and statistically set the enhancement proportions of the grid lines. They could also set an upper area limit for cells featuring Ag grids for which FF of 60% could still be reached.
My stay in ICFO has still not concluded, and so these objectives will be pursued and hopefully some will be reached.

6. AKNOWLEDGEMENTS

I would like to thank Prof. Dr. Jordi Martorell for giving me the opportunity to do this project in the Organic Nanostructured Photovoltaics group at ICFO. It has been an interesting and instructive experience, and the people in group were really welcoming.

Thanks also to Quan Liu for his teaching and helping attitude.

I would like to specially thank my supervisor Paola Mantilla for her support, guidance and teaching, as well as her helpful and nice character.

6. BIBLIOGRAPHY

[1] Smil V. *Energy at the crossroads: global perspectives and uncertainties* 2003, p. 241.

[2] Newport Corporation, http://www.newport.com/Introduction-to-Solar-Radiation/411919/1033/content.aspx.

[3] American Society for Testing and Materials (ASTM) Standard G173-03. Source: http://rredc.nrel.gov/solar/spectra/am1.5/.

[4] S. Xiao and S. Xu, “High-Efficiency Silicon Solar Cells Materials and Devices Physics,” *Critical Reviews in Solid State and Materials Sciences*, vol. 39, pp. 277– 317, Apr. 2014.

[5] Tang C.W. *Appl. Phys*. Lett. 1986, 48, 183.

[6] Haugeneder A., Neges M., Kallinger C., Spirkl W., Lemmer U., Feldmann J., Scherf U., Harth E., Gügel A. and Müllen K. *Phys. Rev.* B 1999, 59, 15346.

[7] Janssen R.A.J., Hummelen J.C. and Sariciftci N.S. *MRS Bull*. 2005, 30, 33.

[8] Halls J.J.M., Walsh C.A., Greenham N.C., Marseglia E.A., Friend R.H., Moratti S.C. and Holmes A.B. *Nature* 1995, 376, 498.

[9] Z. Xu, L.-M. Chen, G. Yang, C.-H. Huang, J. Hou, Y. Wu, G. Li, C.-S. Hsu, and Y. Yang, “Vertical Phase Separation in Poly(3-hexylthiophene): Fullerene Derivative Blends and its Advantage for Inverted Structure Solar Cells," *Advanced Functional Materials*, 2009, vol. 19, pp. 1227-1234

[10] Ning Li and Christoph J. Brabec. *Energy Environ. Sci.*, 2015, 8, 2902

[11] Han, C., Cheng, Y., Chen, L., Qian, L., Yang, Z., Xue, W., Zhan, T., Yang, Y., Cao, W. “Enhanced Performance of Inverted Polymer Solar Cells by Combining ZnO Nanoparticles and Poly[(9,9-bis(3′-(N,N-dimethylamino)propyl)-2,7-fluorene)-alt-2,7-(9,9-dioctyfluorene)] as Electron Transport Layer”, 2016, *ACS Appl. Mater. Interfaces*, v.8, p.3301−3307